escola superior de tecnologia e gestão
instituto politécnico de leiria

Large-Scale Additive Manufacturing for Composites

Master in Product Design Engineering

Patricio Alejandro Banda Vargas

Leiria, November of 2021

escola superior de tecnologia e gestão
instituto politécnico de leiria

Large-Scale Additive Manufacturing for Composites

Master in Product Design Engineering

Patricio Alejandro Banda Vargas

Master's Dissertation held under the guidance of Doctor ESTG Supervisor Fábio Simões, Professor of the Higher School of Technology and Management of the Polytechnic Institute of Leiria and co-orientation of Doctor (s) ESTG Co-Supervisor Artur Mateus, Professor at the Higher School of Technology and Management of the Polytechnic Institute of Leiria.

Leiria, November of 2021

Originality and Copyright

Dedication

I dedicate this work to my mother and father who are my source of inspiration and strength and my brother whose encouragement and love kept me going.

Acknowledgements

First and foremost, I would like to express my earnest gratitude to my primary supervisor, Fábio Simões for his knowledge and immense patience throughout my masters program. I would like to convey my thanks to my secondary supervisor professor Artur Matues for allowing me to contribute on this topic and for offering deep insight into the study.

I am deeply grateful to the research scholars of Center for Rapid and Sustainable Product Development (CDRSP), especially João Vitorino and Hugo Marques, for their assistance and guidance in experiments. I would also like to thank the international and administrative staff of ESTG for all their help in navigating the higher education system in a foreign country.

I would like to extend my sincere thanks to my best friend Anmol Gupta for her help at every stage of this research project. Lastly, I would also like to thank my friends and family for their unwavering support and belief in me.

Abstract

The processability of polymer matrix composites for use in large-scale additive manufacturing was evaluated using fused deposition modeling anchored to a robotic arm. Polypropylene blends were prepared with potato starch, sawdust and calcium carbonate fillers. The surface of the fillers was pretreated in acidic and basic chemical medium. The incidence of particle diameter, chemical pretreatment and amount of plasticizer on the mechanical response of injected specimens was evaluated. The incidence of process variables in large scale additive manufacturing was evaluated through the quantification of geometric deviation and warping of parts printed with the different composite mixtures.

An improvement in mechanical properties was evidenced for those fillers that were chemically treated in a basic medium over those in an acid medium. Wood composites had the closest mechanical properties to those of the matrix, especially those properties related to mechanical strength.

Calcium carbonate composites showed the widest range of processability as well as the best thermal stability, which was evidenced by the lowest geometrical deviation and warping in relation to the other composites.

It was determined that the bed temperature is the factor that has the greatest incidence during the first 6-7 layers of the printing, after this point the environmental temperature factor is the one that controls the heat transfer of the process.

Keywords: Large Scale Additive Manufacturing, Composite Materials, Waste Materials, Wood, Starch, Calcium Carbonate.

Resumo

A processabilidade dos materiais compostos de matriz polimérica para utilização no fabrico aditivo em larga escala foi avaliada utilizando um processo de extrusão associado a um braço robótico. As misturas de polipropileno foram preparadas com partículas de amido de batata, serradura e carbonato de cálcio. A superfície destas cargas foi pré-tratada em meios químicos ácidos e básicos. Foi avaliado o impacto do diâmetro das partículas, do pré-tratamento químico e da quantidade de plastificante na resposta mecânica dos provetes injectados. A incidência de variáveis de processo no fabrico aditivo em grande escala foi avaliada através da quantificação do desvio geométrico e da deformação das peças impressas com as diferentes misturas.

Foi evidenciada uma melhoria nas propriedades mecânicas no caso das partículas que foram tratados quimicamente num meio básico em relação às que que foram tratados num meio ácido. Os compósitos de madeira apresentavam as propriedades mecânicas mais semelhantes às da matriz, especialmente as propriedades relacionadas com resistência mecânica.

Os compósitos de carbonato de cálcio mostraram a maior variedade de processabilidade, bem como a melhor estabilidade térmica, o que foi evidenciado pela mais baixa deflexão geométrica e deformação em relação aos outros compósitos.

Foi determinado que a temperatura de base é o factor que tem maior impacto durante as primeiras 6-7 camadas da impressão, após este ponto o factor de temperatura ambiente é o que controla a transferência de calor do processo.

Palavras-chave: Fabrico Aditivo em Grande Escala, Materiais compósitos, Matérias Primas Residuais, Madeira, Amido, Carbonato de Cálcio.

List of Figures

List of Tables

List of symbols

AAM	Assembled Additive Manufacturing
ABS	Acrylonitrile Butadiene Styrene
AC	Additive Construction
AM	Additive Manufacturing
ASTM	American Society for Testing and Materials
BAAM	Big Area Additive Manufacturing
BJ	Binder Jetting
BSE	Back Scattered Electrons
°C	Degree Celsius
$CaCO_3$	Calcium Carbonate
CC	Contour Crafting
CO_2	Carbon Dioxide
CaO	Calcium Oxide
CDRsp	Centro para o Desenvolvimento Rápido e Sustentavel do Produto
CF	Carbon Fiber
CO2	Carbon Dioxide
CNT	Carbon NanoTubes
CSP	Cable Suspended Platforms
CTE	Coefficient of Thermal Expansion
DED	Directed Energy Deposition
DOF	Degrees Of Freedom
DTA	Differential Thermal Analysis
E	Modulus of Elasticity
ECR	E-Glass Grade
FDM	Fused Deposition Moulding
GF	Glass fiber
LA	Lauric Acid
LSAM	Large Scale Additive Manufacturing
ME	Material Extrusion
MFR	Melt Mass Flow rate
MJT	Material Jetting
MMC	Metal Matrix Composites
ORNL	Oak Ridge National Laboratory
PA	Polyamide
PBF	Powder Bed Fusion

PBT	Poly Butylene Terephthalate
PC	Poly Carbonate
PCT	Poly Cyclohexylenedimethylene Terephthalate
PE	Poly Ethylene
PEEK	Polyether Ether Ketone
PET	Poly Ethylene Terephthalate
PHB	Poly Hydroxy Butyrate
pH	Potential Hydrogen
PLA	Polylactide Acid
PMC	Polymer Matrix Composite
PP	Poly Propylene
PPS	Poly Phenylene sulphide
PS	Poly Sulphone
PS	Poly Styrene
PVC	Poly Vinyl Chloride
RPM	Rotations per minute
SEM	Scanning Electron Microscope
SFRTCs	Short Fiber Reinforced Thermoplastic Composites
SHL	Sheet Lamination
STD	Standard Deviation
STL	Stereolithography
ϵ	Strain
σ	Stress
TGA	Thermogravimetric Analysis
TPE	Thermo Plastic Polyesters
VPP	Vat Photo-polymerization
WCO	Waste cooking Oil
WPC	Wood Polymer Composites
ZnO	Zinc Oxide

Contents

1 Introduction

The advent of additive manufacturing offered new opportunities in the plastic processing industry as layer by layer deposition of material further extended plastic´s capabilities with freedom to design highly complex parts without moulds with a variety of texturing and even usage of multi-materials [1]. Additive manufacturing processes, however were limited to small structures with costly and lengthy development.

The development of large scale polymer additive manufacturing with higher deposition rates and bigger build volumes allowed the creation of huge structures and large parts and components that were previously not possible with AM technologies. However, with the ability of depositing 50 kg of thermoplastic material per hour, these practices can be unsustainable in the long run. That is why it is important to develop alternative composite materials that are made with waste fillers, which can be an eco-friendly way of expanding the raw material while minimising cost and preserving the physical properties of the plastic.

This project will evaluate different thermoplastic composite materials, exploring the possibility of using organic and inorganic fillers to produce pellets for large scale fused deposition modeling. For a baseline, mechanical and thermal tests were conducted on the fillers and matrix. Then the different composite pelletized feed-stock were produced and underwent tests in order to evaluate the mechanical and thermal properties through TGA, DTA and MFR before printing using an extruder mounted on a robotic arm.

1.1 Objective

The main goal is to characterize composite materials physically and mechanically and to relate their properties with their processability and to achieve an effective parametrization of the large scale AM process for non-conventional materials i.e composites based on thermoplastics with added waste products as fillers.

1.2 Work Structure

Chapter 1 Introduction This chapter describes background of the project and its scope. The main objective of this study with which the results will be evaluated has also been defined.

Chapter 2 Literature Review In this chapter, information on the current state of the art of large-scale additive printing technologies has been compiled. Then, taking fused deposition modeling as the selected process, the materials that have been used in different small and large scale additive printing projects in recent years are discussed. The main emphasis has been on composite materials that are filled with waste or natural materials. Information has also been collected on chemical treatments to improve the mechanical and thermal performance of the above mentioned composite materials.

Chapter 3 Materials and Experimental Procedures In this chapter the materials and equipment used for the development of the study have been reported. The experimental techniques used have been described, as well as the first characterization tests of the pure fillers. Thermal processability and MFR values for each of the 15 composite materials prepared and the polymeric matrix have been presented.

Chapter 4 Results and Discussions The mechanical and thermal response for each of the composite materials has been presented in this chapter. Their response has been analyzed in comparison with the pure polymeric matrix. The different parameters of the large-scale printing process such as printing speed, bed temperature, height and width of the bead were evaluated by comparing the variation of geometry and the warping obtained between the different materials.

Chapter 5 Conclusions and Future Works Chapter that presents the most relevant findings of the results, regarding the feasibility of processing the composite materials analyzed in this study for their application in the Big Area Additive Manufacturing process. In addition, future work has been suggested related to the topic raised.

2 Literature Review

2.1 Large Scale Additive Manufacturing

Large Scale Additive Manufacturing (LSAM) is a derivation of Additive Manufacturing (AM), process that is defined by the ASTM as "the process of joining materials to make objects from 3D model data, usually layer upon layer, as opposed to subtractive manufacturing methodologies" [2]. LSAM is a large scale variant of AM. It has lower production cost, higher process speed and higher manufacturing volumes compared to small scale 3d printing technologies. [3]. Labonnote et al. [4], have identified five different technological solutions that have been used for the development of LSAM-related works, projects, and research. These solutions have mainly been developed in the search to overcome the scalability limitation of existing AM technologies. The first developed were gantry solutions, followed by cable-suspended solutions, swarm solutions, multi-purpose robotics, and combination with folding. There are LSAM applications in different fields, such as building, medicine, aerospace, automotive, shipping, energy, among others.

2.1.1 AM technologies

AM is a technology that has been growing steadily since its origin in the 1980s. It has gone from been an experimental technology, to become a dominant technology today, with annual investments of more than 3 billion dollars [5][6]. The seven different AM technologies identified by ASTM in, F2792 that differed in the raw material usage, the energy used to transform material, and in the final product generated are -

- Binder Jetting (BJ), is a technological solution within the AM by using a liquid bonding agent selectively deposit to bond powder particles layer by layer progressively to generate the final shape [7]. BJ technology that presents a build rate of 200 cm^3/min, and large build volumes as long as 0.124 m^3 [8]. Grimm et al. [9] evaluated the final cost of printing a piece with BJ technology, based on its acquisition cost, material cost, maintenance, waste and reprocessing and calculated the effective cost per volume unit at around 0.22 €$/cm^3$.
- Directed Energy Deposition (DED), where the material fed to the process is deposited and melted simultaneously through the application of thermal energy, which generally

comes from a direct source such as a laser, electron or plasma beam. This technology operates with different materials such as ceramics and polymers, however its most widespread application is with metallic powder. Deposition rates of the DED process, ranges between 25-40 g/h were indicated by Gibson, Rosen, and Stucker [10]. Based on this Optomec developed a five-axis hybrid manufacturing system using the LENS process. The LENS 850-R has deposition rates up to 0.5 kg/h for standard steels, titanium, and nickel alloys and has a build volume of 1.21 m^3. Another company, Sciaky developed electron beam based DED machines (EBAM) which utilized wire feedstock. The Sciaky machines have build volumes up to 6m [11].

- Material Extrusion (ME), process that melts filaments of thermoplastic material by applying heat and discharges it through a nozzle to form the piece layer by layer. Go and Hart has determined the deposition rate value for an ME process at 127 cm^3/h for a prototype solution, which is 7 times the average rate of a conventional Fused Filament Deposition (FFD) [12].The effective cost per unit volume was defined as 6.09 €$/h$, for a printer based on this technology [9]. For the build volume, the information available on the Stratasys website was taken as a reference, manufacturer of printers with ME technology, which identifies its Stratasys F900 model as the FFD printer with the highest capacity with a value of 0.5 m^3 [13].

- Material Jetting (MJT), process that creates parts by depositing drops of material through an ink head into a build area, which are stabilized by heat supplied by a light source. According to Gibson et al. [14], MJT technology has droplet sizes ranging from 6μm to 150 μm at rates of 80-100 kHz to 1MHz. It can also have large build volumes as long as 0.4 m^3. Grimm et al. have evaluated the final cost of printing a piece with MJT technology, based on its acquisition cost, material cost, maintenance, waste and reprocessing, calculates the effective cost per volume unit at around 0.62 €$/cm^3$[9].

- Vat Photo-polymerization (VPP) is a process that uses photo-polymers, resins that polymerize by means of light. Gibson et al. [15] have determined the max scan speed value for an VPP process at 25 m/s. The effective cost per unit volume was defined as 1.38 $\$/g$, for a printer based on this technology[15]. For the build volume, the information available on the 3D Systems website was taken as a reference, manufacturer of printers with VPP technology, which identifies its ProX 950 model as the VPP printer with the capacity of value of 0.935 m^3 [16].

- Powder Bed Fusion (PBF) uses a powder that is melted by a heat source, usually a laser. PBF works with different powder materials including polymers (eg. ,Polycaprolactone, Polylactic acid, Polyvinyl alcohol) and its composites (eg. hydroxyapatite / polycaprolactone, calcium phosphate/poly(hydroxybutyrate-co-hydroxyvalerate)), glass, metals (e.g., titanium, aluminium , cobalt) and its alloys (Ti-6Al-4V,AlSi10Mg) [17]. Powder used in process can be recycled to produce more parts [18]. Build rates for PBF process have ranges around to 170 g/h. For the build volume, the information available on the SLM solutions website was taken as a reference, manufacturer of printers with PBF technology, which identifies its SLM 800 model as the PBF printer with the capacity of

0.119 m^3[19]. According to Hopkinson, Hague, Dickens, et al. [20], total costs together with SLS technology are one of the lowest compared to other AM technologies, and in large part it is because this technology allows parts to be stacked one on top of the other thus increasing the number of parts manufactured in each batch. Values around 0.6 €/g were obtained.

- Sheet Lamination (SHL) was one of the first AM technologies commercialized in the 1990s. Sheets of material are stacked, cut and joined together. The cutting of material is usually performed by means of energy provided by a CO_2 laser beam. Grimm et al. [9] have evaluated the final cost of printing a piece with SHL technology, based on its acquisition cost, material cost, maintenance, waste and reprocessing, calculates the effective cost per volume unit at around 25.05 $\$/in^3$. The value is well above the lowest value, an effect generated mainly by the amount of material that is not part of the final piece but it cannot be reused and becomes waste. In the case of the SD 300 pro machine manufactured by Solido, the build volume is equal to 0.0045 m^3 [21]. Build volume rate value for an SHL process at 2.73 h/in^3 for a prototype application were defined [9].

From the previous paragraphs it can be deduced that AM technologies are generally limited to small build volumes (0.03-0.9 m^3), have slow deposition rates (10-185 cm^3/h) and are costly (\$ 100-200$/kg$). Several efforts were made by different companies to solve the aforementioned AM limitations. As a result, new technologies were obtained to increase the build envelope volumes, which fit within the LSAM concept.

2.1.2 LSAM technologies

The five LSAM technologies developed until now are detailed below -

Gantry Gantry is a type of technology that results from the natural scale-up of AM solutions, it is considered as a giant 3D printer. This solution consists of an actuator that is translated through any of the three Cartesian directions X, Y, and Z [22]. The most remarkable gantry-based developments are D-Shape and Contour crafting (CC) as seen in figure 2.1.

Contour Crafting is a process that was patented by the University of Southern California, which has advantages over other AM solutions, such as more high-grade surface quality, faster fabrication rates, and a wider choice of materials. The CC system consists of a gantry system and a nozzle, this makes it possible to produce parts with a larger maximum dimension than those obtained by traditional AM [23]. Initially the process appeared as a hybrid method that combined an extrusion process for molding the object surfaces, and a filling process that built the object nucleus. The smooth and clean exterior surfaces were obtained by

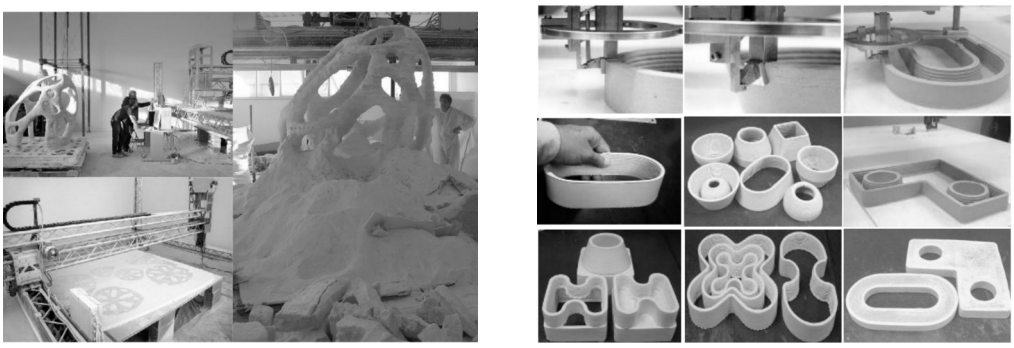

(a) D shape Printing **(b)** Contour Crafting

Figure 2.1: Gantry Technologies

forcing the flow of the extruded fluid through fixed directions using trowels. Khoshnevis [24], have indicated that using this technology a 200 m^2 two-story building can be built in less than 2 days. In contrast of the months it could take using traditional construction methodologies.

D-shape is a process similar to BJ, where a binder is selectively spread along a bed of powdered material. The printing machine is a form of gigantic plotter, equipped with a spraying head which moves along two frames in X–Y axis space. D-Shape is categorized as a gantry-based powder-bed 3D printer that has the ability to print architectural structures with dimensions up to 216 m^3 or more [4].

Cable suspended platforms CSP were created because of the limitations of gantry-type solutions. Constraints that were evidenced when the large and heavy linear axes that are used to delimit the construction were dismantled, and the difficulty of the system to reconfigure the set up shape of the gantry during the construction time [5]. CSP is integrated by an end-effector attached to a frame structure using multiple cables. The end-effector is controlled by motors that can drive the cables in a fully automated way [4]. Bosscher et al. [25] have presented a CSP called “C4 robot", their work cover the stationary and dynamic study of the process, as well as the corresponding cable tensions, to approximate the maximum achievable build envelope of 77440 m^3 a given cube frame structure.

Swarm Swarm approach is a radically different method to gantry solutions, which employ a static physical frame. In this case, small autonomous robots are used that work as a team like "ants" forming a swarm as seen in figure 2.2, hence its name [26]. Ceccanti et al. [27] have determined that a set of small robots in the form of an army worked better than the D-shape technology. These small robots could structures without human intervention, which is not possible in the case of fixed frame installations. The ability to climb through the structure and the communication between the components of the swarm, are the key features required for mini robots to be able to build large structures with unlimited dimensions with a low volumetric capacity.

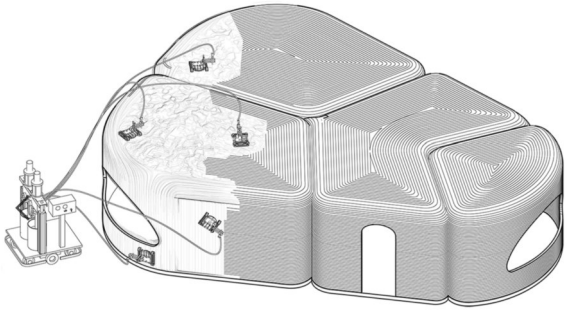

Figure 2.2: Mini-builders Swarm [28]

Assembled Additive Manufacturing AAM is a type of technology under development, which was proposed by Deng and Chen in their study on building thin-shell structures, based on origami. The principle is based on the logic that if a 3D structure is for the first one is higher than in the second case. The critical issues they encountered when they are designed folding structures involved unfolding algorithms of an input model, foldable structure design, and folding mechanism [29].

Robotic arms There are a number of applications that employ robotic arms within the AM industry, as they present solutions to related to geometry, max. reach, or the addition of prefabricated parts on the base structure, among others [4]. Traditional AM solutions are generally limited to three Degrees Of Freedom (DOF), which restricts their applicability. Robotics arms can present 6 DOF (or more in some cases), which gives them the option to perform the printing in a multi-directional way. This allows them to modify the building plane while the layers maintain their planarity [30]. The robotic arms present a versatility in their functionalities, which can range from the extrusion of materials by themselves or be used in auxiliary tasks, such as the addition of additives or help in finishing tasks into the printing process.

In 2014, Oak Ridge National Laboratory (ORNL) in conjunction with Cincinnati Incorporated began to develop a prototype of large-scale polymer, out of furnace, additive printing which would not be controlled by the conditions of a closed chamber [31] (shown in figure 2.3). Under this premise, the concept of Big Area Additive Manufacturing (BAAM) is created, which is a 3D printing technology that can be of the gantry or robotic arm type. It would use polymers in the form of pellets and melt them to create the final structure. With structures with a volume of more than 13 m^3 and deposition rates of more than 10 lb/h of material [32].

BAAM process was the LSAM technology of choice for this research project. The purpose of this work is to extend the existing studies conducted by CDRsp by formulating composite materials, especially those which incorporate any kind of second hand raw materials.

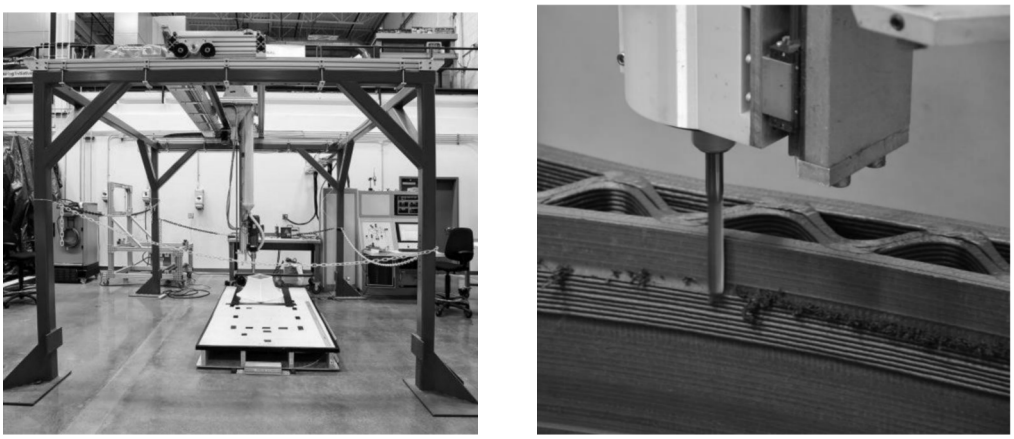

(a) BAAM System at ORNL **(b)** BAAM in situ machining

Figure 2.3: BAAM System [33]

It requires the use of materials that do not deform or distort under the process temperature conditions used throughout the deposition process of the layers that make up the final part, characteristics that are mainly influenced by the coefficient of thermal expansion of the material (CTE) [32].

2.1.3 Materials

Extrusion of thermoplastic materials is widely used within AM, due to several considerations, among which are the market availability and its ease of access to pure materials such as acrylonitrile butadiene styrene (ABS), polylactide acid (PLA), polycarbonate (PC), polyamide (PA) etc. Tekinalp et al. [34] have suggested that pure thermoplastic products represent a limitation within the Fused Deposition Modeling (FDM) process because of their strength and mechanical property restrictions.

In response to this limitation Love [35] studied the impact of carbon fiber (CF) as fillers in an ABS matrix on the mechanical properties and geometric tolerance of FDM printed parts, achieving more than 100% improvement in strength and stiffness for in-plane samples. The geometry of the parts is influenced by the CTE and the thermal conductivity of the material. As CF has a higher thermal conductivity than ABS, it increases the temperature transmission rate of the latter in the system, which in turn generates a reduction in the thermal gradients that, if they are very large, are represented in the final part as deformations. A lower CTE allows reducing the stress in the cooling of the part from its deposition temperature to the environmental equilibrium, generating a complementary effect.

Love and Duty [36] have evaluated a mixture of materials such as ABS, 13%CF-ABS and highlighted the importance of anisotropy of materials within the BAAM process. Hill et al. [31], have studied 32 different material samples in which the base material was ABS and the main

fillers were virgin and recycled CF in different proportions, they also employed Glass Fiber (GF) as filler. Duty et al. [3] have studied the impact of extrusion on the mechanical properties of parts printed by BAAM with composite materials, concluding that the mechanical properties in the direction of the printed plane are almost similar to those obtained as a reference by an injection process for pure and composite materials, while in the direction of the y and z planes the properties of the composite materials fall drastically in relation to the reference values, due to the loss of adhesion between deposited layers and the influence of the fillers on the porosity of the body of the printed part. Gandha et al.[37] have fabricated a magnet made of anisotropic Nd-FeB+Sm-Fe-N composite material on nylon, obtaining encouraging results. Pigliaru confirms the results obtained by Gandha even changing the matrix to PEEK [38].

2.1.4 Design and operation parameters

Gibson et al. [39] have mentioned in the chapter *Design for Additive Manufacturing* four characteristics of AM. The first is Shape Complexity that is in theory any shape could be developed without any limitation. Second, is Hierarchical Complexity which says that variations in the complexity of the shape can be made at different scales and could be combined to form the final figure. Third, Functional Complexity which says it is possible to manufacture entirely functional structures, i.e. not only parts of a structure but a complete and functional structure. And fourth, Material Complexity, which refers to the fact that different materials can be used throughout the structure, either at specific points or in different layers.

Most of the limitations and advantages of small-scale AM apply to BAAM. Below is a list of specific design and operation parameters where this technology has been used that, being a developing area of study, many are still under investigation [39]:

- Bead width is the thickness of the bead that the nozzle deposits. The bead width not only depends on the nozzle diameter but also can be varied by adjusting print or extruder speed. According to Roschli et al. [40] design structures that have bead widths thicker than 2 inches should be avoided and recommends that sections with more thickness should be printed in multiples also known as slicing.

- Cavities is a hollow space surrounded by a solid body. In BAAM, as they are large structures, they normally do not contain support material, so these cavities must be self-supported by the structure of the printed figure. In the case of using support material, all the necessary space for the machinery to enter to remove it must be considered [40].

- Bridges are over hangs that are connected to the parts on both sides. It is aspect to evaluate in the design of structures with BAAM, unlike small-scale AM technologies where

the large ratio of surface area-to-volume ratio allows the material to solidify immediately after extrusion, in BAAM this ratio is much lower, so depending on environmental conditions and the type of material, warping and possible fracture of the structure may occur due to the slower solidification of the extruded material [41].

- Overhang angle is the angle formed between the parallel line of the external face of the printed figure and the base line where it was printed is known. In the case of BAAM, since it is an AM technology outside the oven, this represents a greater challenge since no support material is used for the structures. Crespo identified that the structure can be self-supporting even with angles less than 30º with respect to the vertical [42]. Roschli limits the printing for structures with an angle less than 40º with respect to the vertical, since below this value the contact surface between layers is drastically reduced and leads to structural failures [40]. Similarly, the position where the extrusion nozzle starts and ends plays an important role in the tolerance of this design parameter, it has been determined that it is better to start and end the extrusion at the same point in each layer to reduce variations in bead adhesion caused by time variations between layers.

- Resolution is linked to the thickness of the layers [43], a better definition is achieved with less thickness and lower height but alongwith the need for a greater number of layers to replicate a structure. Leading to consequent increase in construction time and additional costs that this action entails. For BAAM printed structures this trade off between build resolution and build rate is especially critical, since as can be deduced from the following equations the deposition rate drops with the square of the increase in resolution [44]. For printing at a coarse resolution, the layer height is designated by h. A typical bead profile on BAAM has a 2:1 aspect ration of width to height. Thus, the cross-sectional area of a bead is given by:

$$a_c = 2h^2 \tag{2.1}$$

The print speed is designated as v. This gives the following for deposition rate in volumetric flowrate:

$$Q_c = a_c v = 2h^2 v \tag{2.2}$$

If the layer height is divided by n for a fine resolution print, the cross-sectional area of the bead now becomes:

$$a_f = 2\left(\frac{h}{n}\right)^2 = 2\frac{h^2}{n^2} \tag{2.3}$$

The print velocity is assumed to remain constant. Thus, the following is found for the volumetric flowrate of a fine nozzle:

$$Q_f = a_f v = 2\frac{h^2}{n^2} v \tag{2.4}$$

Now the deposition rate for fine and coarse prints can be compared:

$$\frac{Q_f}{Q_c} = \frac{2\frac{h^2}{n^2}v}{2h^2v} = \frac{1}{n^2} \tag{2.5}$$

Print with high output and with a high resolution is the challenge to overcome. Two solutions have been explored, first is to increase the printing speed, a solution that has physical limitations, such as the acceleration and deceleration capability of the printer, and process limitations such as the minimum layer time, which represents the minimum necessary cooling time between layers so as not to compromise the mechanical performance of the structure due to the lack of stiffness in one layer to support the next layer during the printing process [40]. Shah et al. [45] have mentioned the possibility of dynamically changing the layer thickness according to the complexity of the figure, because it has been evidenced that in vertical planar geometries the incidence of layer thickness is minimal, while in curved shapes it is necessary to use a smaller layer thickness that allows to increase its detail.

To generate this dynamic division of layers, solutions such as those proposed by Ultimaker or Slic3r optimize the relationship between throughput and resolution. The printing of structures with different layer thicknesses can be executed by changing the nozzle during printing by using rotatable keys attached to the nozzle or by several extruders depending on the need and availability, this adaptation in the printing system increases its complexity and therefore its operation and maintenance costs. It is recommended that the thickness of the larger layers be a multiplot of the smaller ones.

- Warping is caused by internal stresses generated by the temperature gradients between the deposited material and the nozzle, the allowable temperature difference between layers between the ends is according to the following equation [46].

$$\frac{dT}{dz_{max}} = \frac{8\delta}{L^2\alpha} \tag{2.6}$$

One way to counteract warping is by conditioning the air that circulates around the printing area, with the idea of reducing the temperature gradient that is the cause of this phenomenon, for prints of small length a hot bed is sufficient, however for longer surfaces may be insufficient, being necessary to implement air conditioners to raise the temperature of the room, which can cause problems with electronic equipment sensitive to high temperatures, in addition to ergonomic problems in the staff working in these areas [45].

Due to the complexity of the BAAM process there are different variables that are correlated with the printing quality of a part using this technology, being a process under development, advances are still being explored both in its design and operation in the search to solve the challenges presented.

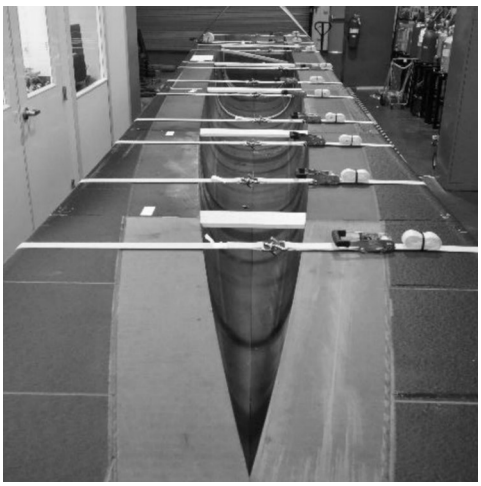

(a) Mold for a boat [47]

(b) Skeleton node for a wind turbine naecelle [48]

Figure 2.4: Applications of BAAM

2.1.5 Applications

BAAM is a new technology that started to be developed 7 years ago at ORNL laboratories, differentiating itself from traditional AM by exceeding its processing speed by 1000X, increasing the size of the fabricated parts by a factor of 10X, and showing a cost reduction by a ratio of 100X [36].

Hover, a renewable energy company printed scaled versions of wind tunnels major and minor diverters parts for wind tunnel testing [49]. Within the same industry and with feedback from previous work, ORNL in collaboration with Vestas Wind Systems was able to develop skeleton nodes for wind turbine naecelle , justifying the use of BAAM for a clean energy economy [48]. The examples can be seen in figure 2.4.

ORNL in partnership with Alliance MG, LLC (AMG) decided to collaborate with the idea of developing a ready-to-paint boat mold without the need for additional coatings generated by the finishing limitations of BAAM. The result was successful and resulted in improved manufacturing costs and lead times over the traditional process [47].

Another industry, where BAAM has shown potential for development is the construction industry. Mold as seen in figure 2.5 (a) were printed for the construction a building façade made of precast concrete. These molds were produced on site and had longer life of up to 200 uses compared to the 20 uses of traditional wood molds. Molds with complex geometries that would take much longer to produce with the traditional method of wood and the manual skill of an operator, can be developed by BAAM [50].

For the generation of energy, magnets are needed, which with the passage of time and

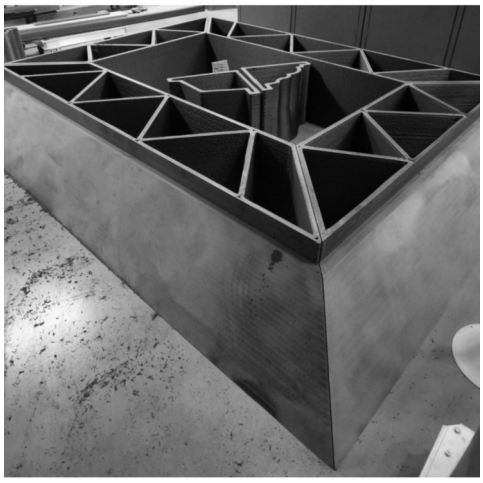

(a) Assembled concrete mold of four individual pieces [50]

(b) Printed Body installed on Jeep [52]

Figure 2.5: Applications of BAAM Industry

the improvement of technology have been varying their size and structure being increasingly smaller and complex, and it is in this complexity where the AM finds its differentiation factor compared to other manufacturing processes of magnets such as injection. Li et al. [51] have presented BAAM as a suitable method for the effective fabrication of bonded magnets, which present any shape with minimum cost and waste.

For military applications, ORNL used to print a carbon fiber model of a 1953 Willy's Jeep war car as well as a metal bumper made from mild steel and aluminium wire [52] as seen in figure 2.5 (b). This work was based on lessons learned from previous work on a prototype Shelby Cobra-type car [53].

Whirlpool Corporation in collaboration with ORNL evaluated the opportunity to employ BAAM for the development of foam cooling cabinet molds for their products, which are normally complex to produce because of all the associated sub-processes. The results lead to overall reduced build times [54].

2.2 Thermoplastic - Matrix Composite Materials

A composite material is one that is made up of a mixture of two or more materials that differ in composition and interact at a macroscopic level with recognizable interfaces between them. There is a continuous phase or binder called matrix and a discontinuous phase or reinforcement, which can be present in the form of particles or fibers. The traditional function of reinforcement, as its name indicates, is to reinforce the matrix material and improve its structural properties, so they are generally stiffer and stronger than the continuous phase.

However, there are other types of materials that can be added and are called fillers, mostly used in polymeric systems, which have various justifications, such as cost reduction or improvement of strength, deformation or thermal conductivity properties, among others [55].

Polymer-Matrix Composites (PMC) are the most developed composite materials and the ones that have experienced the greatest interest and applications over the years. Their matrix can be formed by thermoplastic or thermosetting polymers. The toughness and stiffness of this type of composite is closely linked to the mechanical properties of the fiber, while the matrix aids load distribution, prevents aging and corrosion.

The main advantages of PMCs are that they can be processed by conventional plastics processing techniques, with a ratio of low cost and high processing volumes, in the case of thermoplastic PMCs they can be easily reshaped. Their main disadvantage is their high CTE values, which generate severe internal stresses in the composite, compromising its structure. The most commonly used thermoplastic matrix materials are polyolefinics (polyethylene, polypropylene), vinylic polymers (polyvinyl chloride (PVC)), polyamides (PA), polyacetals, polyphenylenes (polyphenylene sulphide (PPS)), polysulphone and polyetheretherketone (PEEK). The most common thermoset polymer matrix materials are polyesters (unsaturated), epoxies and polyi-mides [56].

2.2.1 Thermoplastic matrices

There is a wide variety of thermoplastic polymeric matrices that are used in industrial applications, mainly because their use is associated with a reduction in manufacturing costs, higher toughness and tolerance to imperfections if their are compared with thermoset polymers. As they are mostly partially crystalline polymers, their physical and mechanical properties can be affected during processing due to the variation of heating or cooling conditions that directly affect temperature gradients [56]. Different thermoplastic matrix can be employed depending on the application and its demands, some of them are detailed below.

Thermoplastic Polyesters (TPE) There is a wide range of organic chemicals that fall under the denomination of polyesters, with a wide variety of industrial applications such as injection molding, blow molding of bottles and oriented films. Polyesters have good chemical and solvent resistances [56] [57].

- Polyethylene terephthalate (PET) PET applications for the processing of parts by AM have been developed using neat or recycled PET as a matrix in conjunction with filler materials forming composite materials, Ahmed [58] have presented the behavior of rPET filled with GF by printing different parts with complex geometries, varying the proportion of filler used. The use of continuous-phase PET and dispersed-phase PP

to form copolymers in the quest to increase the amount of processable semicrystalline thermolastics by fuse deposition has been planned by Chatham et al. [59].

- Poly(butylene terephthalate) (PBT) origin was motivated by the expiration of PET patents, manufacturers in the quest to keep extending the protection of their innovation and profits looked for the polymerization of other polyalkene terephthalates and came up with PBT. Gnanasekaran studied the fabrication of PBT composites filled with graphene and Carbon Nanotubes (CNT) achieving complex geometries, highlighting the selection of PBT over other thermoplastic polymers due to its ability to obtain highly functional as well as mechanically robust structures [60].

- Polyamides (PA) globally known as Nylon, is a crystalline thermoplastic with high modulus, strength, and impact properties; low coefficient of friction; and resistance to abrasion. Its main applications are in the textile industry in the manufacture of fibers, it is also used in the manufacture of packaging. If aromatic groups are placed in the backbone of Nylon, the so-called aromatic polyamides are formed, whose main commercial exponents are Kevlar and Nomex [56] [57]. Dickson presents in his study the mechanical behavior of Nylon reinforced with CF, GF and Kevlar for its application in the printing of parts by means of AM, highlighting that the tensile strengths of the composites were superior to that of aluminum [61].

- Polysulphone (PS) are a group of amorphous, transparent aromatic thermoplastics with T_g of around 185 ºC. It is used when good resistance to high temperatures is required, such as in the case of coffee chambers or the internal coating of microwave ovens, or sterilization equipment.

- Polyether ether ketone (PEEK) belongs to the family of polyether ketones. Their characteristics make it suitable for applications in the aeronautical and military industries [56] [57]. Stepashkin et al. performed structural and thermal analysis of FDM printed parts using PEEK reinforced with CF fibers, comparing the behavior of the printed part with its cast counterparts [62]. Mys proposed the use of Polysulphone pellets for its subsequent transformation into powder form for the use in Selective Laser Sintering, achieving due to the absence of extensive warpage allows multilayer tests to be performed in the form of tensile bars for mechanical characterization, obtaining values below the expected and that were mainly associated with the porosity of the printed specimens [63].

- Polyphenylene sulfide (PPS) is part of this group of polymers, it presents high temperature resistance, with a melting point of 287 ºC, high strength, and high chemical resistance due to the presence of benzene and sulfur ring in its backbone. Liu et al. [64] have studied rheology, crystal structure, and nanomechanical properties in large-scale additive manufacturing of polyphenylene sulfide/carbon fiber composites, raising the importance of variable anisotropy in understanding the dependent geometry of molecular arrays and the resulting properties of the AM component.

2.2.2 Fillers

Fillers materials are particles that are added to a matrix to improve specific properties. When their addition improves mechanical properties, they are called reinforcements. If they do not generate any improvement in the mechanical performance then they are called inert fillers or extenders. Main motivation for such fillers is generally cost reduction.

These enhancements are influenced by different specifications, such as the particle diameter, its geometry, distribution in the matrix or the chemical interaction of its surface with the matrix. The chemical interaction between the contact surfaces of the filler and matrix is what dictates the level of adhesion between the parts and the consequent mechanical response of the system [56] [57].

There is a variety of fillers and there is no single classification for them. According to their geometry, they can be classified between amorphous and regular shaped. According to their morphology they are classified into particles, fibers. More generally, if their composition and chemical origin are considered, they can be divided into organic and inorganic fillers.

Next, a brief description of the fillers used in this work is presented, divided according to the previously mentioned classification of chemical origin, with applications and investigations that have been developed using these components. Finally, certain physical and chemical treatments that have been employed to improve the mechanical, physical, chemical or electrical response of the fillers within the composite materials in which they have been used are detailed.

Organic

Sawdust a natural organic compound with a composite structure in which cellulose (50-60%) is surrounded by lignin (25%) and hemicellulose. Cellulose is a polysaccharide with a large number of hydrogen bonds, which makes it very soluble in water. Cellulose is a natural polymer characterized by its high strength and stiffness per weight unit. Hemicellulose is the component that forms the structure blocks, generic name used to refer to the set of heteropolysaccharide compounds of natural origin present in the structure of wood. Lignin is a three-dimensional amorphous polymer with phenol propane-based, acts as water sealant in the stems and helps in controlling water transport through the cell wall. Lignin is considered to be the cement that binds or covers the spaces between the polysaccharide chains [65]. Wood Polymer Composites (WPC) are composites that have wood as a dispersed material in a polymeric matrix. Commonly used polyolefins are polyethylene PE [66], polypropylene (PP) [67], polyvinyl chloride PVC [68], polystyrene (PS) [69] and acrylonitrile butadiene styrene (ABS).

The advantages of WPCs are their low density, cost savings, biodegradability, easy processing, high versatility and productivity. While the main disadvantages are related to its limited thermal stability for temperatures above 220ºC, the lack of homogeneity in the dispersion of fibers or particles in the matrix, which leads to the use of additives that help to improve the surface interaction between the components. The most common way of using wood in composites is by means of the so-called wood flour, which is finely sieved wood in the form of granules with the appearance of flour, hence its name. The main characteristics of wood flour are bulk density around 0.1-0.3 g/cm^3. Specific gravity is about 1.3-1.4 g/cm^3 [70] [71].

While cellulose provides positive effect on mechanical and other properties of the composite material (such as decreased coefficient of thermal expansion-contraction, etc.), lignin generally makes the product weaker, easily burn in the course of processing and release CO_2 and other gaseous products, making the product density lower, and greatly accelerates fading of the WPC after outdoor exposure. This is why different treatments have been employed in the quest to make the effects of cellulose predominate over those of lignin [65].

One treatment method is delignification, which is the extraction of lignin from wood, based on the higher chemical affinity of lignin with polar solvents such as water or alcohols. This reaction is carried out by means of chemical agents or solvents, in the first case it can be carried out by means of alkalis or acids, being the one that uses basic alcohols the most known and industrially used is the denominated Kraft process. Complex process, which consists of the treatment of lignocellulosic materials with Kraft pulping liquor.

This kraft pulping liquor is composed of sodium hydroxide and sodium sulfide, and other sodium salts in smaller quantities. The process that uses organic solvents for lignin extraction is known by the generic name of Organosolv, this reaction is carried out as seen in figure 2.6, having different qualifications depending on the type of organic compound used, having its main advantages over the Kraft model in cost reduction and the possibility of reusing the extracting solvent, which makes it a more sustainable process [72].

Mirmehdi, TONOLI, and Dabbagh [73] have evaluated the influence of delignification, filler content and filler type in the preparation of lignocellulose-polyethylene composites observing an improvement in the mechanical properties of the delignified fibers. The Thermal behavior of extracted and delignified pine wood flour was analyzed by Chen, finding that the composites containing the delignified particles presented the lowest thermal stability compared to their similar ones that went through the extraction process [74]. Other process parameters that have been evaluated in order to improve the adhesion beztween the components have been the pH, where Dimitriou Dimitriou, Hale, and Spear [75] concluded that the surface activation of the delignified wood flour with hydrogen peroxide is higher at a medium basic pH.

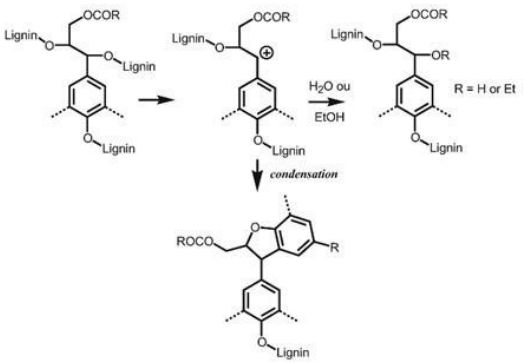

Figure 2.6: Organosolv Delignification [72]

Starch is a natural, highly hydrophilic granular polymer with amylose (20-30%) and amelopectin (70-80%) as its main constituents. It has been widely used as an additive in food, paper and paint industries, among others. In the search for more environmentally friendly solutions in the manufacture of petrochemical derivatives, starch has been finding new spaces either as an additive, for example in polyethylene sheets to help their biodegradability, or as a filler where Poly(lactic acid) PLA is the preferred matrix for its mechanical properties [76].

Starch is a brittle and thermally sensitive product which restricts its use. Improvements in the performance of its mechanical and thermal properties have been planted by varying different process and compositional parameters. Olaiya et al. evaluated PLA-Chitin-Starch blends at different concentrations, concluding that the PLA-chitin-starch blend has the best mechanical properties compared to PLA-chitin and PLA-starch blends [77]. The structure and oxidative degradation of starch-Polyethylene composites was studied by Khar'kova, identifying a reduction in the decomposition temperature of these composites relative to pure composites independently, as well as an improvement in the modulus of elasticity and elongation at break [78].

The brittleness of starch and its composites, elongation range 5 to 10%, has been extensively evaluated in the literature. One way to improve the processability, elongation and inter-molecular mobility of the compounds is by the amount and type of plasticizer used in the polymerization reaction. A good plasticizer should be chemically compatible with the polymer to yield a stable, homogeneous mixture [79]. The use of used cooking oil from sunflower seed fried oil as a plasticizer for starch composites with PLA was proposed by Volpe, obtaining as results that replacing a percentage of glycerol with edible sunflower seed oil, especially if fried, as a plasticizer for the starch results in an improvement in thermal stability and mechanical properties of the material [80].

Lubis ran a set of tests in which he evaluated composites of mango seed starch with nanoparticle zinc oxide as filler and ethylene glycol as plasticizers, varying the concentrations of the filler and plasticizer, obtaining the mixture of nanoparticle ZnO concentration

6% and ethylene glycol 25% the best response to mechanical tests. The effect of varying the amount of lauric acid on the thermal and mechanical properties of polyhydroxybutyrate (PHB)/starch composite biofilms was studied by Adorna, concluding that the thermal and mechanical properties in the case of elastic strain of the films increased with the addition of LA, although the tensile strength decreased compared to pure PHB/S [81], which agrees with that expressed by Ke, who in his case used triethyl citrate as plasticizer.

Inorganic

Calcium Carbonate Inorganic compound of mineral origin widely used in the polymer industry, of chemical formula $CaCO_3$ and molecular weight 100 g/mol, Specific gravity between 2.7-2.9 g/cm^3, with linear coefficient of thermal expansion from 2 to 6 x 10^{-6} 1/ºF. It occurs naturally as sedimentary rocks and is separated into chalk, limestone, and marble. It is generally considered that mineral type fillers increase the modulus but elongation and impact strength are drastically reduced [65] [70], information that coincides with different investigations, one of them by Piekarska, where he evaluated the thermal and mechanical properties of polylactide (PLA) composites with different grades of calcium carbonate [82]. Another study evaluated the effect on the mechanical properties of composites with epoxy matrix and $CaCO_3$ as filler, and concluded that the mechanical properties, such as flexural modulus, and fracture toughness of composite were enhanced by the addition of cube-like and rod-like $CaCO_3$ nanoparticles [83].

It has been reported that in some cases, the calcium carbonate may be treated to improve interaction with the hydrophobic thermoplastics, mainly when seeking to reduce the polarity of this hydrophilic compound, and thus reduce the interaction between filler particles [84]. For several reasons, including price and market availability, stearic acid as a surfactant has been used to improve $CaCO_3$ hydrophobic properties, Mihajlović et al. [85], have defined the mechanism that calcite employs to adsorb stannic acid and based on that study Cao et al. [86], have proposed to evaluate the incidence of chemical surface modification of calcium carbonate particles with stearic acid using different treating methods, where he employs either a "wet" or a "complex" method to treat the stearic acid that is contacted with the filler, before being mixed with a high density polyolefin, concluding that "wet" and "complex" treated $CaCO_3$ composites have a higher tensile strength than their untreated and "dry" treated $CaCO_3$.

Glass fiber GF is born from an amorphous material such as glass, whose main constituent is silica sand, which in mixture with limestone, boric acid, and other ingredients that are dry-mixed, melted (at approximately 1260°C), and then drawn into fibers. Fibers that are widely used as reinforcing materials in composite materials, and have undergone constant development, as a result of which different types of GF have been obtained, of which the

Table 2.1: Properties of Glass Fiber (GF) [56]

Type	Nominal tensile modulus $GPa(lb/in^2 10^6)$	Nominal tensile strength $MPa(lb/in^2 10^3)$	Ultimate strain %	Fiber density $Mg/m^3(lb/in^3)$
E	72.5 (10.5)	3447 (500)	4.8	2600 (0.093)
R	85.2 (12.5)	2068 (300)	5.1	2491 (0.089)
Te	84.3 (12.2)	4660 (675)	5.5	2491 (0.089)
S-2	86.9 (12.6)	4585 (665)	5.4	2550 (0.092)

most commonly used as filler is the E-glass grade (ECR glass) which adds calcium aluminosilicate compounds to the base structure of the GF to make it chemically resistant and has mechanical properties as presented in table 2.1, values that may vary depending on the supplier and the type of surface treatments or coatings applied to the fiber [56] [71].

These coatings allow the GF to improve its adhesion properties with the matrix and protect the filler from possible damage during processing, commonly known as finish or sizing and are specific to each supplier and the final application of the fiber. Kiss et al. [87] had studied glass fiber roving sizings and yarn finishes in high-performance GF-PA6 and GF-PPS composite laminates and determined that by varying the filler coating, mechanical properties of the composites can be improved. As a result of the adhesion of the fibers with the matrix. Sherif et al. [88], have concluded that the mechanical and thermal behavior of polysulfone (PSU) composites was positively influenced by the thermal treatment previously applied to the fibers, supporting this variation in the modification generated by the treatment in the fiber coating.

The increase in the application of materials called Short-fiber-reinforced thermoplastic composites (SFRTCs), which include composites with GF fillers, in industries such as automotive, household appliances, construction, among others, has posed a new challenge to the sustainability of this type of products, due to their complexity in order to recycle them. Several studies have focused on the evaluation of the effects of recycling, reuse or reprocessing after primary use. Pegoretti reviews the main challenges and opportunities and presents the current state of the art on the recycling of SFRTCs, highlighting the coincidence between studies on the degradation of the molecular weight of the polymer matrix and the rupture of the fibers as a consequence of reprocessing, despite which it is concluded that the mechanical properties are in most cases preserved to acceptable levels until 6 to 10 reprocessing cycles [89].

2.3 Chapter Outcomes

Below is a summary of all the key points explored in this chapter:

- The processability of a material used in the FDM process is related to the degree of crystallinity of the material, its CTE and its thermal conductivity. If the crystallinity of the material is decreased by adding fillers that in turn increase its thermal conductivity and reduce the CTE, the result will be less deformation of the extruded part.
- Composite materials with wood in their matrix have shown an improvement in their mechanical response by removing the lignin from their matrix, a chemical compound that makes the product weaker, burns easily in the course of processing and releases CO_2 and other gaseous products.
- It has been reported that in some cases, calcium carbonate can be treated to improve the interaction with hydrophobic thermoplastics, mainly when seeking to reduce the polarity of this hydrophilic compound, thus reducing the interaction between the filler particles.
- Starch is a brittle and thermally sensitive product, which limits its use. Improvements in the performance of its mechanical and thermal properties have been achieved by varying different process parameters and composition.
- The influence of the chemical medium on the adhesion of fillers with polymeric matrices has been evaluated, taking into account the implication of this parameter on the degree of activation of the surfaces in contact, finding higher adhesion at a basic medium.

3 Materials and Experimental Procedures

This chapter contains the procedures and techniques that were used to prepare the different batches of composite materials, which were then characterized and evaluated for their potential application in the manufacture of parts using BAAM technology.

Figure 3.1 indicates the procedure followed for the elaboration of this degree work. The filler materials were selected taking into account their origin, and their degree of availability for application in the printing of a defined geometry by means of BAAM.

The fillers were chemically treated in different chemical media of different concentrations and with different chemical reactions depending on the case. After the treatment, a processability profile was elaborated using the TGA, MFR test. The morphology of the fillers was determined by SEM technique. Once independently characterised, the composites were prepared in different proportions by mixing the fillers with the polypropylene 961 matrix.

Mechanical tests were performed on injected specimens for each of the composites in order to evaluate the composites. Measurement of the melting and solidification temperatures as well as the latent enthalpies of the composite materials were carried out.

A square with a cross-sectional area equal to 150 x 150 mm was printed using the BAAM process. Temperature and time data were collected to make a temperature profile of the process at different operating conditions. A mathematical model was applied to evaluate the incidence of different operating parameters and compare it with the experimental data obtained. Finally, a qualitative evaluation of the match between the printed parts in relation to the part obtained with the pure matrix material was carried out.

3.1 Materials

A polymeric matrix and three fillers, two of natural origin and one inorganic, were the materials used for the realisation of this project. The properties and characteristics of the materials used are detailed below.

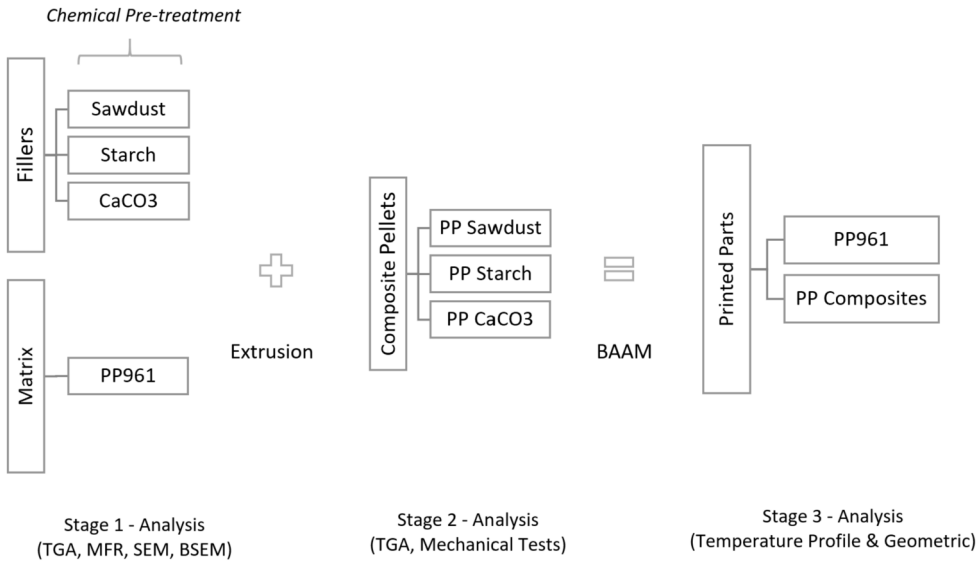

Figure 3.1: Experimental Procedure

3.1.1 Polymeric matrix

The matrix selected for the preparation of the composite materials was polypropylene (PP) of Bormod (BE961MO) brand, whose properties are presented in table 3.1.

Table 3.1: Properties of Bormod- BE961MO

Property	Nominal Value Unit	Test Method
Density	0.905 g/cm^3	ISO 1183
Melt Mass Flow Rate (MFR) (230ºC/ 2.16Kg)	12 g /10 min	ISO 1133
Tensile modulus	1200 MPa	ISO 527-1/50
Tensile Stress (Yield)	23.0 MPa	ISO 527-2/50
Tensile Strain (Yield)	5.3%	ISO 527-2/50
Flexural Modulus	1250 MPa	ISO 178
Heat Deflexion Temperature 0.45 MPa Unannealed	92.0 ºC	ISO 75-2/B

3.1.2 Composite Fillers

The group of fillers comprised of sawdust, potato starch and calcium carbonate, also know as stone powder, were chemically treated on their surface to evaluate their impact on the mechanical, physical and thermal properties of the composites.

3.2 Experimental techniques for characterization and equipment

3.2.1 Melt Mass-Flow Rate (MFR)

This test is based on ISO 1133 or its equivalent in ASTM D1238 "Standard Test Method for Melt Flow Rates of Thermoplastics by Extrusion Plastometer", which allows to calculate "the rate of extrusion of molten thermoplastic resins using an extrusion plastometer. 6MBA Melt Flow System from Ray-Ran Test Equipment Ltd. was the equipment used for this experiment. After a specified preheating time, resin is extruded through a die with a specified length and orifice diameter under prescribed conditions of temperature, load, and piston position in the barrel" [90]. The result is reported in grams of material flowing in 10 minutes.

Procedure A specified within the standard was used, and the test was applied to each of the polymeric materials according to the suggested load weight and temperature conditions.

3.2.2 ThermoGravimetric Analysis (TGA)

TGA is a thermal analysis technique, which finds its main application in the determination of the thermal stability of a compound by measuring the ratio between the solid and gas phase of the system over a temperature range defined by the person performing the analysis within a controlled atmosphere [91]. This technique was used both in the fillers independently, in order to identify the thermal behavior of each one of them and to verify their applicability in the formation of polymeric composite materials, from which, in addition to their thermal behavior profile, the melting and crystallization temperatures and their phase change enthalpies were extracted. The equipment used was the Simultaneous Thermal Analyzer (STA) 6000 from PerkinElmer with a controlled inert atmosphere of molecular nitrogen.

3.2.3 Scanning Electron Microscopy (SEM)

Technique based on the principles of optical analysis, where a beam of high frequency electrons is emitted on the structures of interest and generates different responses depending on the morphology, chemical composition and crystallinity of the samples analyzed [92].Analyses were performed by scanning electron microscopy/energy dispersive spectroscopy (Zeiss, MERLIN, Field Emission Scanning Electron Microscope-Gemini II/Oxford Instruments, X-MAXN) at 10kV. This technique was used to obtain the morphology of the isolated fillers and fillers inside the polymeric compounds, to observe the degree of dispersion of the fillers throughout the polymeric matrix. In the case of the fillers that varied their hydrogen potential, the back scattered electrons (BSE) were also used to identify this variation.

3.2.4 Mechanical Tests

Tensile and bending properties of the composites were tested according to the procedures specified in ASTM D638 'Standard Test Method for Tensile Properties of Plastics', and ASTM D790 'Standard Test Methods for Flexural Properties of Unenforced and Reinforced Plastics and Electrical Insulating Materials'. Values of Modulus of Elasticity (E), Stress (σ), and Strain (ϵ) were obtained for each of the prepared mixtures by means of these tests and in conjunction with the thermal behavior, a ranking of potential materials that were used for the fabrication of parts by means of BAAM was determined. The equipment used for tensile and bending test was Zwick z100

3.2.5 Printing with BAAM

Figure 3.2: Robot Extruder

The equipment used for the printing of the parts by means of the large-scale AM technology was the articulated robotic arm of 6 degrees of freedom of the YASKAWA HP20F brand, which has a maximum reach length equal to 1717mm, available at CDRsp. The robotic arm was controlled by a compact MOTOMAN FS100 controller - figure 3.2. The selected polymer composite pellets were placed in the feeding hopper of the robotic arm and the specified geometry was reproduced by means of the G-code of the robot. In the process of evaluating the impact of the operating parameters on the reproduction fidelity of the printed part, different parameters such as deposition speed, interlinear layer height, deposition bed temperature and certain environmental conditions were varied.

Table 3.2: Materials and operating conditions - Delignification reaction.

Material /Equipment	Quantity (g)		Concentration		Range appreciation	
	Acid	Basic	Acid	Basic	Acid	Basic
Ethanol	442.15	413.79	99.8%	99.8%		
Evaporated water	1252.77+251.72	1251.12+266.9				
Wood (sawdust)	337.11	350.85				
Sulfuric Acid	23 ml		1 [mol/l]			
Ammonium Hydroxide		10 ml		1 [mol/l]		
Balance					± 0.01 g	± 0.01 g
PH meter					± 0.01 [H*]	± 0.01 [H*]
Stove					± 1ºC	± 1ºC
Heater + Stirrer			900 rpm		± 50 ºC | 50 rpm	± 50 ºC | 50 rpm
Thermometer					± 1ºC	± 1ºC

3.2.6 Wood delignification

Wood delignification reaction helps a more homogeneous distribution of the fillers as indicated in the previous chapter, the chemical medium in which the reaction was carried out was varied between acid and basic, so that the impact of this variable on the mechanical properties of the derived composite materials could be evaluated. The process diagram can be found in Appendix A. The sawdust was placed in an oven at 50ºC for 72 hours, during which time the organic matter reduced its moisture content. Then the dried dust is sieved to separate the particles and differentiate it according to its particle diameter. The particle diameter were between the range of 500 to 1000 μm and 300 to 500 μm. The shape of the particles does not have a defined figure, however as main characteristic it can be highlighted that its length is greater than its diameter and thickness, having a rectangular or cylindrical aspect as shown in figure 3.3.

Once the dehydrated sawdust was sieved, the particles with the largest diameter were chosen to receive the chemical pretreatment. The smaller ones were separated and did not receive the chemical bath. This was done in order to evaluate the incidence of particle diameter, and the presence or absence of chemical treatment as variables in the performance of their corresponding composite materials in the mechanical and thermal tests performed in the following sections.

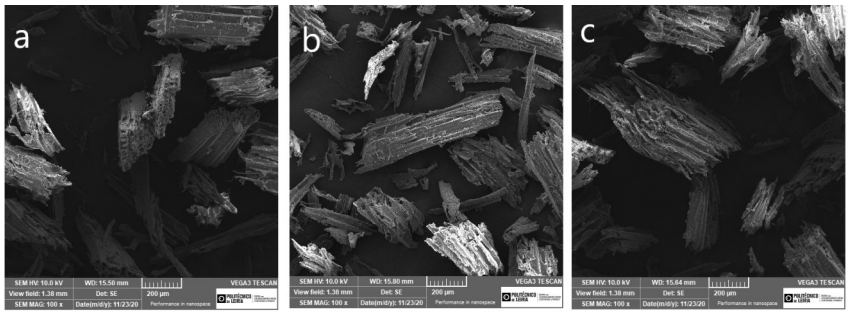

Figure 3.3: SEM - Wood Chips a) Basic treatment b) Neat c) Acid

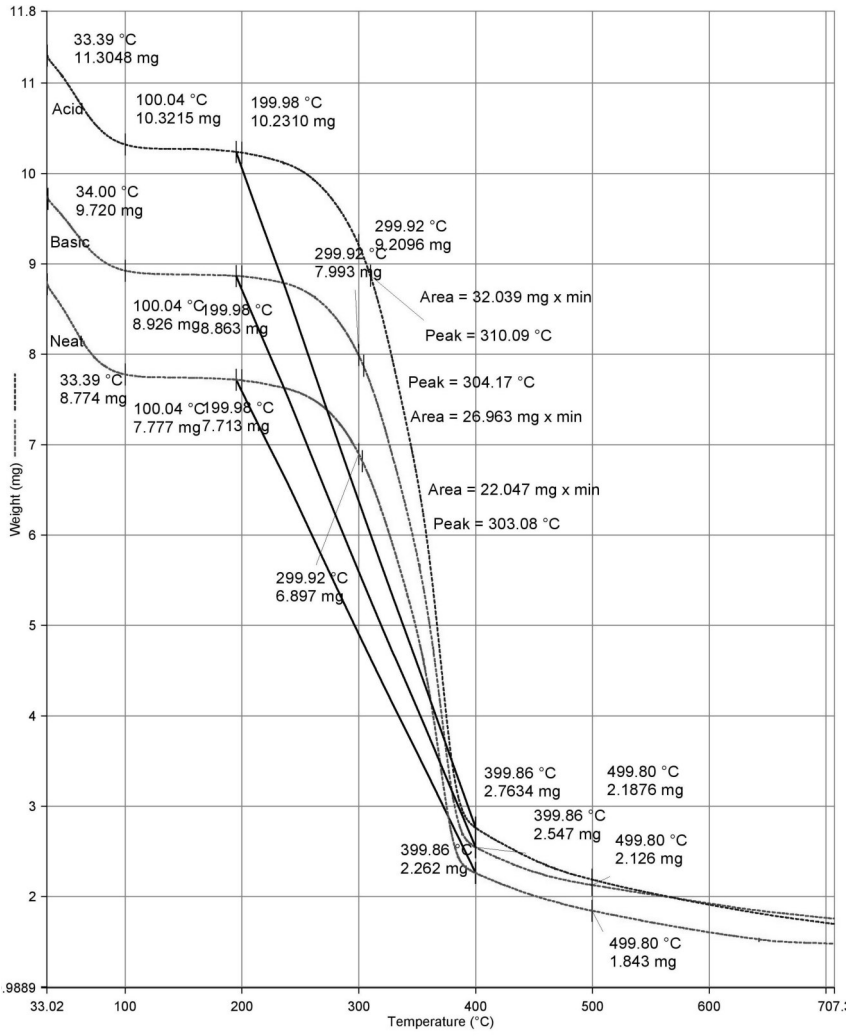

Figure 3.4: TGA - Wood Sawdust a) Neat (Red) b) Basic medium (Green) (c) Acid medium (Blue)

The materials and operating conditions used for the delignification reaction of the wood sawdust that was mixed with the polymeric matrix in the extrusion process are mentioned in table 3.2. As sawdust is an organic filler, when it is exposed to temperatures above 200ºC, it can generate significant mass losses due to changes in the chemical structure.The heating rate inside of the TGA equipment was 10ºC/min up to 750ºC. with which the behavior of the filler at different temperatures was analyzed, evaluating its change of composition in the defined temperature range.

Figure 3.4 shows the behavior of sawdust throughout the temperature range between 35 and 750ºC. In general, a similar behavior is observed in the slopes generated for sawdust in its different presentations, but a more detailed analysis shows table 3.3, which indicates the percentages of organic matter lost throughout the defined temperature range due to heat.

The first slope is in the range of 35 to 100 ºC with losses between 8 and 11.3% with

Table 3.3: Analysis of weight losses and degradation temperatures of sawdust

Treatment	dp	Wo (Intial Weight)	Wi (Weight Loss)				
	(µm)	(mg)	(%)	(%)	(%)	(%)	(%)
Neat	300	8.77	11.36	12.09	21.39	74.22	78.99
Basic	500	9.72	8.17	8.82	17.77	73.80	78.13
Acid	500	11.30	8.70	9.50	18.53	75.56	80.65
	T(ºC)	34	100	200	300	400	500

untreated wood showing the highest losses. In the first range the losses are associated with the elimination of the free water that is part of the sawdust composition.

The next slope to consider is the one presented in the range of 200 to 300 ºC where the sawdust loses between 18 and 20% of its initial weight, it is at this point where the hemicellulose of the wood degrades, amorphous component and that precedes in degradation to the cellulose that begins to degrade when passing the peak of the curve that is around 300ºC.

From this point the slope is much steeper and between 300 and 400ºC up to 75% of the organic matter is lost, where after 350ºC the lignin begins to decompose, a component that was removed from the samples with chemical treatment (acid and basic) and is evidenced by the prominence of these slopes in the indicated range. It is concluded from this analysis that the sawdust filler in its different presentations has thermal stability up to temperature values close to 300ºC.

3.2.7 Partial Crystallization

In the previous chapter the benefits of using inorganic materials as reinforcement materials in polymeric matrices were detailed. In the case of calcium carbonate, different works have studied its impact on the physical, mechanical and thermal properties of the composite materials in which this type of filler is part of.

The incidence of the chemical treatment of calcium carbonate together with stearic acid in wet medium was evaluated, by using the partial crystallization reaction of used cooking oil (WCO) in different chemical concentration media (acid, basic), forming an oleogel which was subsequently added to the polymeric matrix and combined in the extrusion process.

Partial crystallization is the chemical reaction that generate a geometric reorientation in the fats molecules to improve their physical and chemical properties, like palm stearin, a hard fraction obtained by palm oil dry fractionation. It is mixed with other fats to improve tolerance to high temperatures, and for crystal morphology and stability [93]. However, blending with

polyunsaturated soft oils (like sunflower,soybean or rapeseed oils) remains necessary in order to impart plasticity to the partial crystallized product. A wide range of consumer table margarines and spreads, bakery margarines and frying shortenings can be formulated by mixing interesterified blends and native oils in adequate proportions.

Prior to the partial crystallization reaction, the stone powder was placed inside an oven at 50ºC for a period of time of 72 h, to later visualize its morphology through the SEM technique. Figure 3.5 shows an irregular morphology of the component and a particle diameter of less than 5μm and with accumulations of particles in certain places due to the hydrophilic capacity of the material.

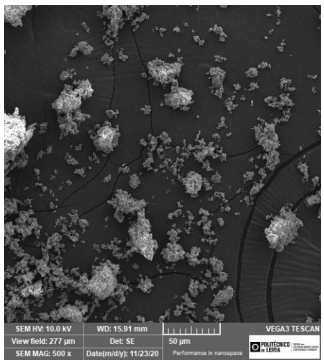

Figure 3.5: SEM - $CaCO_3$ neat

The materials and operating conditions used for the partial crystallization reaction of used cooking oil with stearic acid to form the oleogel, that was mixed together with calcium carbonate and the polymer matrix in the extrusion process, are listed on table 3.4.

Table 3.4: Materials and operating conditions - Partial Crystallization of WCO reaction.

Material / Equipment	Quantity (g)		Concentration		Range appreciation	
	Acid	Basic	Acid	Basic	Acid	Basic
Stearic Acid	30	30	97%	97%		
Waste cooking Oil (WCO)	300	300				
Sodium Hydroxide	5 ml	5 ml	12.5 [mol/l]			
Sulfuric Acid	1		1 [mol/l]			
Ammonium Hydroxide		1		1 [mol/l]		
Balance					± 0.01 g	± 0.01 g
PH meter					± 0.01 [H*]	± 0.01 [H*]
Heater + Stirrer			900 rpm	900 rpm	± 50 ºC | 50 rpm	± 50 ºC | 50 rpm
Thermometer					± 1ºC	± 1ºC

The partial crystallization reaction was carried out in acid and basic medium, by implementing chemical agents that allowed modifying the concentration of ions in the reaction medium. This was done in order to evaluate, if any, the incidence of this factor in the mechanical properties of the polymeric composite with calcium carbonate filling. The procedure of this reaction can be found in Appendix A.

In order to analyze the thermal behavior of calcium carbonate over a defined temperature range, the TGA technique was applied to evaluate, if any, the compositional changes in the component and its percentage variation over the range. The heating rate was 10ºC/min up to 950ºC.

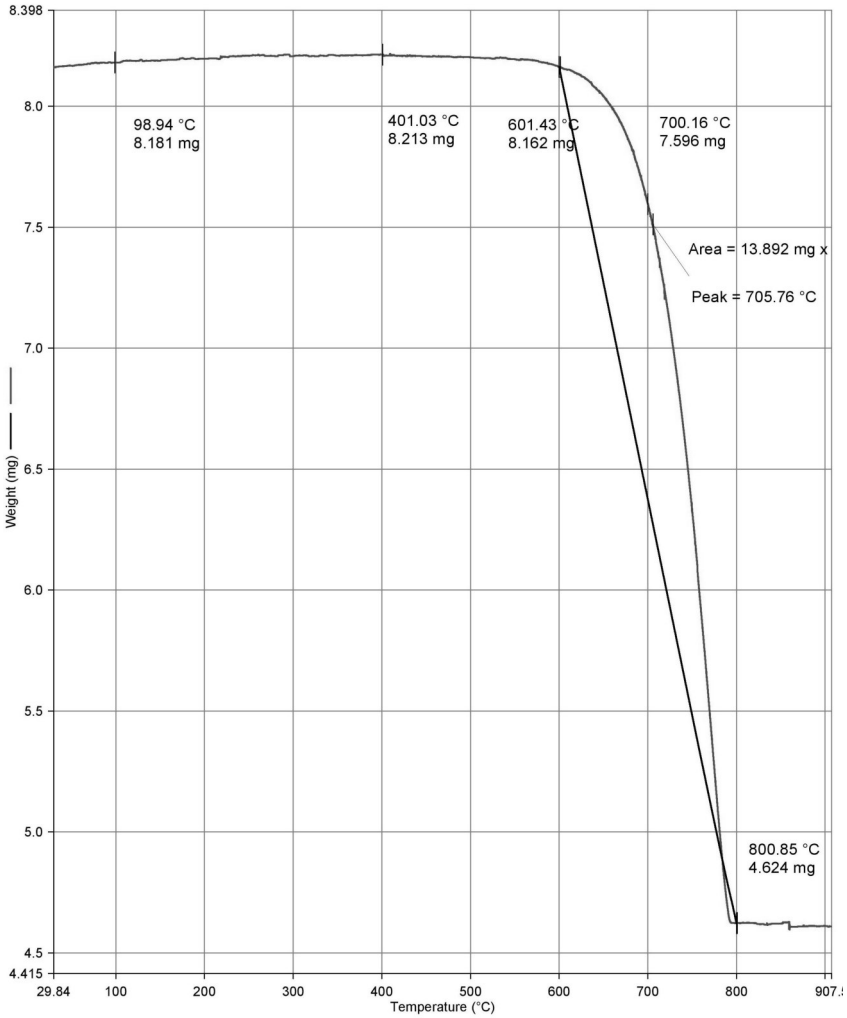

Figure 3.6: TGA $CaCO_3$ (stone powder)

Figure 3.6 shows the behavior of calcium carbonate over the temperature range between 35 and 950ºC. In general, a curve with a single temperature peak at around 705ºC is observed, and it is from this point that the slope of the curve becomes steeper. Since calcium carbonate is an inorganic component, its resistance to heat degradation is much higher than the other fillers used in this study, which are organic compounds such as sawdust and starch. Between the range of 35ºC and 600 ºC there is no major variation in the composition of the stone powder, when passing this first range, a degradation begins to occur in the calcium salt called thermal decomposition or calcination in which the salt gives way as products to its base oxide (CaO) and the release of CO2 in gaseous form.

The calcium salt has a molecular weight of 100 g/mol of which 40% corresponds to the chemical element calcium, which corresponds to the remaining matter after 750ºC as shown in table 3.5. It is concluded from this analysis that the pure calcium carbonate filler has thermal stability up to temperature values close to 700ºC.

Table 3.5: Analysis of weight losses and degradation temperatures of calcium carbonate

Treatment	dp	Wo (Intial Weight)	Wi (Weight Loss)				
	(μm)	(mg)	(%)	(%)	(%)	(%)	(%)
Neat		8.74	-	-	0.06	6.99	43.38
	Tº(C)	34	100	400	600	700	800

Stearic acid was added to the calcium carbonate as an additive in the form of oleogel, which originated from its reaction with used cooking oil in a chemical reaction of partial crystallization in a humid medium, system in which its chemical potential state was varied between acid and basic. As previously performed with the calcium salt, the TGA analysis of the stearic acid oleogel in acidic and basic media was performed in order to see the behavior of the system composition over a defined temperature range. The heating rate was 10ºC/min up to 500ºC.

Figure 3.7 shows the behavior of the oleogel derived from the partial crystallization reaction between stearic acid and used cooking oil. The red line representing the oleogel with basic treatment and in blue the compound with treatment in acid medium. When the used vegetable oil is mixed with a saturated fatty acid, the first loss observed in the figure 3.7, are in the range between 35 and 100ºC, possibly caused by the release of volatiles. After this loss, the decomposition of the triglycerides into their basic units of composition, which are fatty acids, carboxylic acids, ketones, alcoholic groups and other compounds that are thermally degraded, triggering the rupture of the chains of the compounds and eliminating carbon dioxide in the form of gas as well as molecular hydrogen.

After 250ºC the slope begins to steepen until around 360ºC, which is the peak of the curve, coinciding with the boiling point of stearic acid, and from this point until 400ºC between 38 and 45% of the initial matter is lost. After 400ºC and reaching 500ºC the amount of mass lost exceeds 80% as shown in table 3.6. It is concluded from this analysis that the additive stearic acid, used in a chemical reaction with used cooking oil that gives rise to an oleogel in its different presentations, has a thermal stability up to temperature values close to 350ºC.

3.2.8 Polymerization Reaction

A polymer is formed by a chain of monomers of the same type that can be associated with other compounds along this chain. In the case of starch, the monomers that generate the biopolymer through the polymerization reaction are amylase and amelopectin, In both cases, for the reaction to take place, the presence of a plasticizer material is necessary, which acts

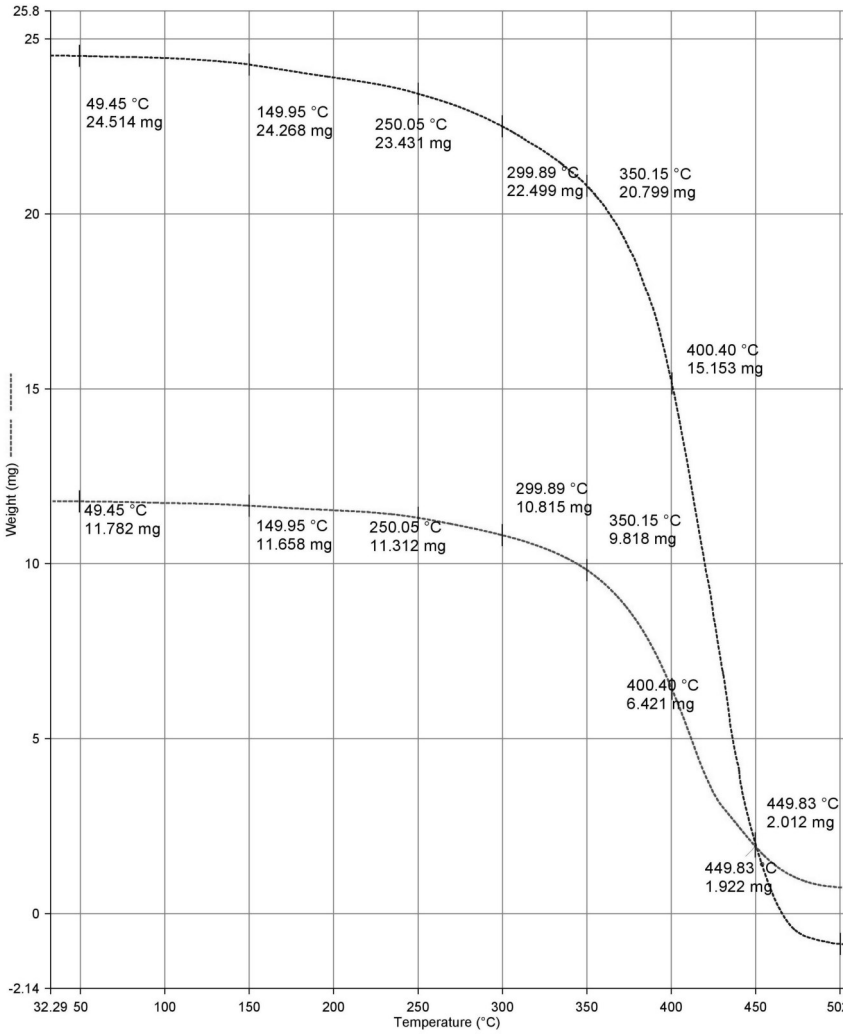

Figure 3.7: TGA Stearic Acid Oleogel a) Basic - Red b) Acid - Blue

as a means of reducing the forces between the hydrogen bonds that hold the polymer chains together. In this work, the aim is to demonstrate the influence that the variation of the amount of plasticizer can have on the polymerization reaction prior to its homogenization by extrusion with a polymeric matrix.

The particle of pure potato starch, brand "Cimarron", was characterized by observing its shape and size through the SEM technique in which it was defined that the particle shape is oval and that its diameter is between 25 to 50 μm as can be seen on figure 3.8.

Table 3.7 lists the materials and operating conditions were used for the polymerization reaction of potato starch with the plasticizer (glycerin) for the formation of the starch polymer, which was adhered to the polymeric matrix after the extrusion process. It is noticeable that the only variation in the composition of the material for the reaction is determined by the amount of plasticizer used.

Table 3.6: Analysis of weight losses and degradation temperatures of stearic acid oleogel

Treatment	dp	Wo (Intial Weight)	Wi (Weight Loss)					
	(µm)	(mg)	(%)	(%)	(%)	(%)	(%)	(%)
Basic	-	11.792	1.14	4.07	8.29	16.74	45.55	83.70
Acid	-	24.514	1.00	4.42	8.22	15.15	38.19	91.79
	T(ºC)	50	150	250	300	350	400	500

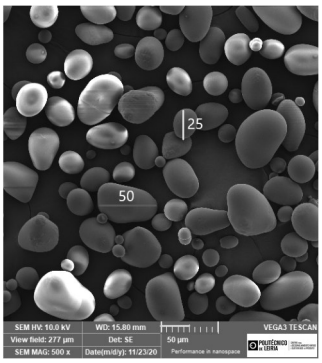

Figure 3.8: SEM-Potato Starch

The polymerization reaction is a chain reaction in which the monomers are coupled one after the other and give way to a chain called polymer. In the case of potato starch used in this work, the amount of plasticizer used varied, being equal to 30% or 15% in mass ratio with respect to starch, as indicated in the procedure located in table 3.7.

- The amount of anhydrous glycerol required for the reaction was weighed, 60 g for the mixture with 30% glycerol content in relation to the amount of starch, and 30 g for the mixture with 15% glycerol content.
- The glycerin was heated for 15 minutes at a controlled temperature of 80°C and with a stirring speed equal to 200 rpm.
- Once the stipulated time had lapsed, the starch was added into the glycerin's flask, it was left to react for 5 minutes maintaining the same temperature conditions, the stirring speed was reduced owing to the increase in viscosity of the mixture.
- It was left to cool, and the starch polymer was removed with the help of a spatula since it solidified and adhered to the walls of the flask

Potato starch is a natural component that can be biodegraded under normal conditions of pressure and temperature, therefore its importance lies in the ability to generate more environmentally friendly polymers.

Table 3.7: Materials & Operating conditions Polymerization Reaction of potato starch with Glycerin

Material /Equipment	Quantity (g)		Concentration	Range appreciation
	10-30	10-15		
Glycerol	60	30	86-89%	
Starch	200	200		
Balance				± 0.01 g
Heater + Stirrer				± 50 ºC | 50 rpm
Thermometer				± 1ºC

As part of the study, the behavior profile of the system at different temperatures was defined to define the ranges in which it can be processed in order to guarantee its mechanical, physical and chemical properties, this was done using the TGA technique presented in figure 3.8. The heating rate was 10ºC/min up to 550ºC.

Table 3.8: Analysis of weight losses and degradation temperatures of potato starch (Brand: "Cimarron")

		Initial Weight	Weight Loss					
Sample	dp (µm)	Wo (mg)	Wi (%)	(%)	(%)	(%)	(%)	(%)
Starch	25-50	13.175	15.10	17.85	17.79	34.69	71.27	75.79
	T(ºC)	33	100	200	250	300	350	400

Table 3.8 shows the analysis of the behavior of potato starch subjected to heating under a controlled atmosphere and in a temperature range between 35 and 550ºC. Two marked slopes are evident, the first one being the one between 35 and around 100ºC, where a weight loss of up to 15% is reached, loss related to the free water inside the system, The next point that marks a new drop in the amount of solid matter present in the system is around 250ºC, which is the point where the degradation of the main components of starch, such as amylose and amylopectin, begins, up to 350ºC, at which point a weight loss of 71% was obtained, with a maximum peak reaction rate located at 303ºC. Once 400ºC was exceeded and with a weight loss of around 75% of the initial value, the organic matter continued to decompose until the ash and salts of inorganic compounds remained as remnants. It is concluded from this analysis that the sawdust filler in its different presentations has thermal stability up to temperature values close to 250ºC.

3.3 Composite Materials

For all three fillers, the extruder was set up under recommended feed rates and temperature conditions. The mixtures were homogenized in their different proportions, to obtain the pellets that will be used in the following processes. The operating conditions used in the extruder

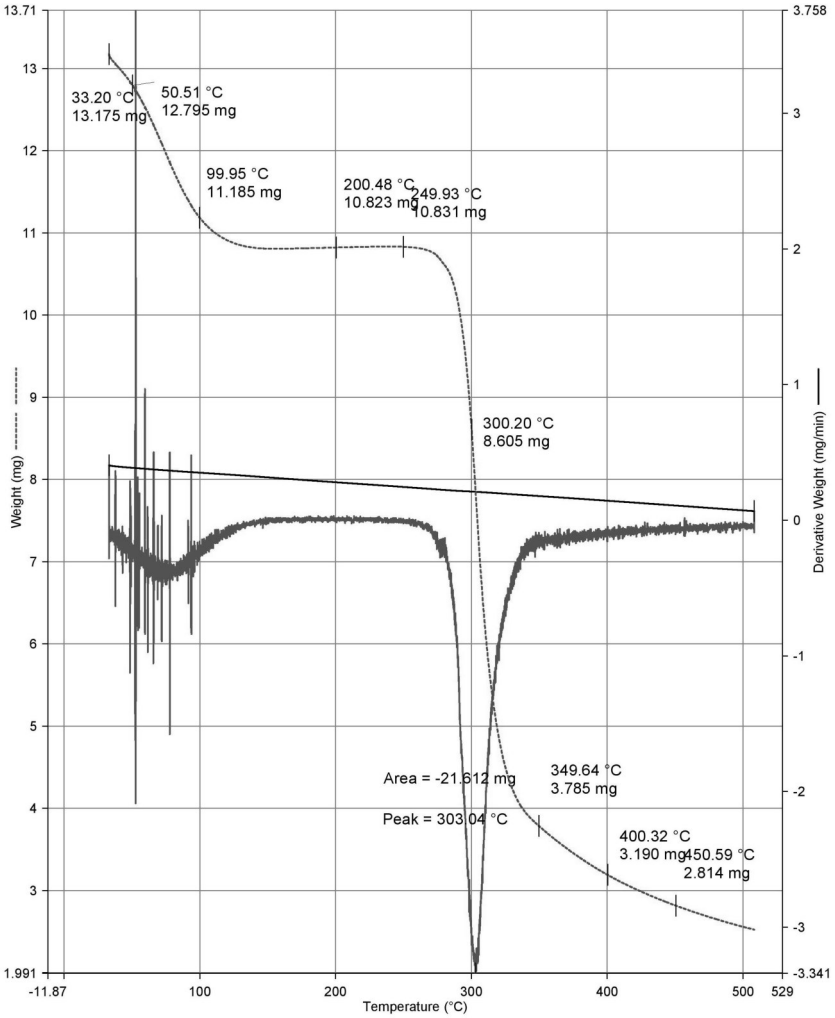

Figure 3.9: TGA Potato Starch Pure

are referenced in table 3.9. The filaments resulting from the extrusion were placed inside a grinder, it was configured to work at a processing speed in the range of 25 to 45 rpm.

For each of the fillers, a range of mass percentage was defined and pellets produced accordingly.

3.3.1 Sawdust

Sawdust was combined with the PP961 polymer matrix within an extruder and the extruded filaments were pelleted for each mixture, with the proportions indicated in table 3.10. The ratio between the filler and the matrix was varied between 5 and 10%, for each of the prepared fillers, in order to verify the incidence of this variable on the thermal and mechanical properties

Table 3.9: Extruder Operating Conditions

Conditions	Units	Fillers		
		Sawdust	$CaCO_3$	Starch
Feeding Speed	rpm	0.2	0.2	0.2
Extruder Screw Speed	rpm	65	45	65
Temperature	ºC			
Zone 1		195	205	195
Zone 2		200	210	200
Zone 3		205	215	205
Zone 4		210	220	210
Zone 5		210	220	210
Zone 6		-	-	-
Zone 7		205	215	205
Zone 8		205	215	205
Zone 9		200	210	200

of the composite polymer.

Table 3.10: Mass Balance of Materials: Sawdust - PP composite

Material	Quantity (kg)		
	Neat	5%	10%
Polypropylene	X	X	X
Sawdust acid medium (500μ)		Y=X/20	Y=X/10
Sawdust basic medium (500μ)		Y=X/20	Y=X/10
Sawdust neat (300μ)	Y=X/20		

3.3.2 Calcium Carbonate

Calcium carbonate was combined with the PP polymer matrix within an extruder and the extruded filaments were pelleted for each mixture, with the proportions indicated in table 3.11. The ratio between the filler and the matrix was varied between 5 and 10%, besides the amount of oleogel applied in each sample varied between 25 and 10% in relation to the amount of filler used in each of the prepared fillers, in order to verify the incidence of these variables on the thermal and mechanical properties of the composite polymer.

3.3.3 Starch

Starch was combined with the PP polymer matrix within an extruder and the extruded filaments were pelleted for each mixture, with the proportions indicated in table 3.12. The ratio between the filler and the matrix was kept at 10%, while the amount of plasticizer used in

Table 3.11: Mass Balance of Materials: Calcium Carbonate - PP composite

Material	Quantity (kg)			
	10-25%	10-10%	5-25%	5-10%
Polypropylene	X	X	X	X
CaCO3	Y=X/10	Y=X/10	Y=X/20	Y=X/20
Acid Oleo gel	Z=Y/4	Z=Y/10	Z=Y/4	Z=Y/10
Basic Oleo gel	Z=Y/4	Z=Y/10	Z=Y/4	Z=Y/10

the preparation of the starch polymer was varied between 15 and 30%, for each of the prepared fillers, in order to verify the incidence of this variable on the thermal and mechanical properties of the composite polymer.

Table 3.12: Mass Balance of Materials: Starch - PP composite

Material	Quantity (kg)	
	10-30%	10-15%
Polypropylene	X	X
Starch	Y=X/10	Y=X/10
Glycerin	Z=3Y/10	Z=3Y/20

3.3.4 Melt Mass Flow Index Composite Materials

Even though MFR is not a fundamental property of the materials, it allows to have a general idea of their rheology through the characterization of the uniformity and amount of creep of the material under controlled standard conditions. Table 3.13 presents the MFR values obtained experimentally for each of the 15 mixtures prepared for this study. In addition, the value of the polymeric matrix PP961 is equal to 12.6 g. Value that could be interpreted as signal of lower molecular weight of the matrix in relation to its composite derivatives. Graph 3.10 shows the MFR values for the different groups of fillers used. Calcium carbonate formed composites were the ones with the lowest fluidity index compared to the others. While this is not a definitive result, it shows a higher thermal stability of those materials when their have been heated and subjected to shear forces such as those present in the FDM process. Those composites that have wood in their matrix and additionally received chemical treatment in their filler particles present a lower MFR than those in which the added particles were not chemically treated and have a smaller particle size.

Table 3.13: MFR Composites Materials

Material	MFR (g/10 min)	STD (g/10 min)	Error (%)
PP 961	12.6	0.54	2.1
PP + 5% WT Wood (300u)	10.6	0.18	1.2
PP+5% Acid Wood (500u)	10.7	0.29	1.9
PP + 10% Acid Wood (500u)	9.0	0.74	5.6
PP + 5% Basic Wood (500u)	9.5	0.31	2.2
PP + 10% Basic Wood (500u)	7.3	0.42	3.9
PP + 10-15% Starch-Glycerin	6.3	0.12	1.3
PP + 10-30% Starch-Glycerin	7.8	0.42	3.7
PP + 5-10% Acid CaCO3	5.7	0.39	4.7
PP + 5-25% Acid CaCO3	5.2	0.31	4.1
PP + 10-10% Acid CaCO3	5.5	0.26	3.3
PP + 10-25% Acid CaCO3	5.8	0.16	1.8
PP + 5-10% Basic CaCO3	5.5	0.34	4.2
PP + 5-25% Basic CaCO3	6.1	0.38	4.3
PP + 10-10% Basic CaCO3	5.7	0.21	2.6
PP + 10-25% Basic CaCO3	5.9	0.15	2.1

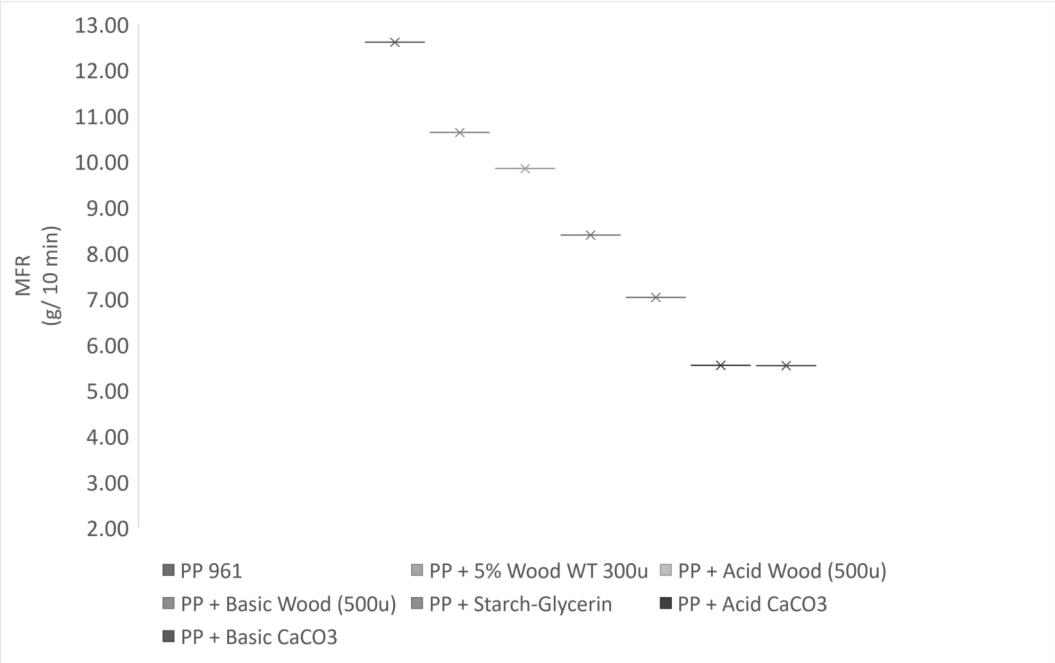

Figure 3.10: Mass Melt Flow Rate - Group

4 Results and Discussions

This chapter presents the results of the evaluation of processability of polypropylene matrix composites for application in BAAM. Firstly, mechanical tests results of each of the composites are presented. This was done to measure the influence of particle diameter, chemical pre-treatment and plasticiser amount on the mechanical response. Next, a set of thermal analyses of both the composites and the LSAM process are presented. These tests were carried out in order to obtain the relationship between the different parameters of the process.

4.1 Mechanical Tests

Tensile and bending tests were performed on each of the mixtures prepared for evaluation. The incidence of particle diameter, chemical pre-treatment and amount of plasticiser were evaluated, considering the pure matrix as a reference value.

4.1.1 Bending tests

Table 4.1 shows the individual values of the mechanical properties obtained after the bend test for each of the composite materials. In the case of wood-based fillers, there are no major variations between them; however, those with a chemical preparation in a basic medium show a slight advantage of 1-2% over those prepared in an acid medium or with a particular diameter of 300μm.

For compounds with starch as a filler in their matrix, the average value of Flexural modulus is around 94% of the value of the pure matrix. However, looking at the individual values of each compound, it can be seen that for the PP + 10-15 Starch-Glycerin mixture, the Flexural modulus values are practically equal to those of the pure matrix. It should be noted when increasing the amount of plasticiser (glycerol) in the mixture, the values decrease by 12%.

From the figure 4.1 it can be seen that all the composite components that were subjected to the mechanical bending test do not exceed the value of Flexural modulus of the virgin material (PP961) which is equal to 1.1 GPa, presented in orange colour in the figure. As the

Table 4.1: Bending Mechanical Test Result

Material	Mean Flexural Modulus (MPa)	STD Flexural Modulus (MPa)	Error (%)	Mean Flexural Stress (MPa)	STD Flexural Stress %	Error (%)
PP 961	1111.06	89.30	2.8	37.38	2.25	2.1
PP + 5% WT (Wood 300μ)	1046.91	64.11	2.3	32.05	1.22	1.4
PP+5% Acid Wood (500μ)	1040.58	65.92	2.4	28.35	2.07	2.8
PP + 10% Acid Wood (500μ)	1061.38	69.97	2.3	29.04	1.27	1.5
PP + 5% Basic Wood (500μ)	1023.43	32.23	1.4	28.25	1.17	1.8
PP + 10% Basic Wood (500μ)	1104.35	66.05	2.3	32.26	1.10	1.3
PP + 10-30% Starch-Glycerin	976.38	110.41	4.0	29.91	2.92	3.4
PP + 10-15% Starch-Glycerin	1109.85	119.94	4.8	33.72	2.43	3.2
PP + 10-25% Acid CaCO3	917.12	26.88	1.2	31.01	1.20	1.6
PP + 10-10% Acid CaCO3	996.62	43.13	1.6	33.59	0.86	1.0
PP + 5-25% Acid CaCO3	926.45	44.99	2.0	32.44	1.59	2.0
PP + 10-25% Basic CaCO3	1076.40	63.88	2.4	36.69	1.85	2.1
PP + 5-10% Acid CaCO3	971.98	56.19	2.2	33.08	1.56	1.8
PP + 10-10% Basic CaCO3	1041.85	55.46	2.2	33.29	0.93	1.1
PP + 5-10% Basic CaCO3	1028.24	19.03	0.8	33.60	0.22	0.3
PP + 5-25% Basic CaCO3	1100.81	91.03	3.4	35.02	1.84	2.1

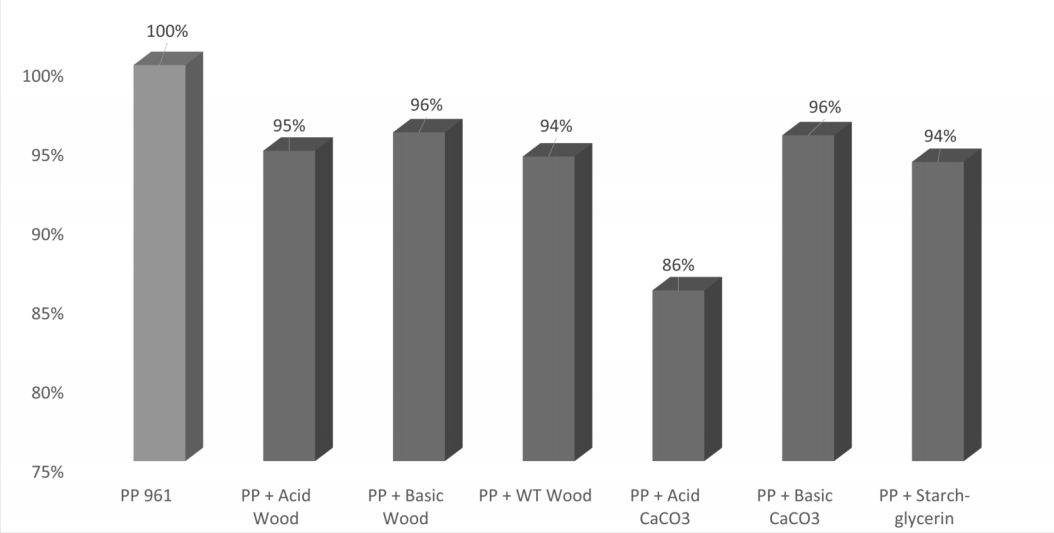

Figure 4.1: Flexural Modulus Group

flexural modulus is an indicator of the resistance of a material to deformation when exposed to bending stresses, it was determined that the stone powder composites in an acid medium were the ones that presented the lowest resistance with a value of 86% compared to the pure matrix.

It is interesting to note that materials with the same inorganic filler mentioned above and varying their chemical conditioning in a basic medium prior to extrusion obtained a value of 96% of the value of the matrix. In the individual values presented in table 4.1, it can be observed that in both acidic and basic medium for the inorganic filled composites, the flexural modulus value increases with increasing amount of oleogel present in the mixture.

Figure 4.2 shows that all the composite components that were subjected to the mechanical flexural test do not exceed the value of flexural strength of the virgin material (PP961) which is equal to 37.4 MPa, presented in orange colour in the figure. The resistance to deformation generated by bending stresses presented by the composites with matrix filled with the mixture of calcium carbonate with oleogel treated in different chemical media were the ones that presented a higher resistance with values between 87 and 93% compared to the pure matrix. Those containing in their composition the chemically treated oleogel in a basic medium showed the highest value. As in the case of the flexural modulus, those in which the amount of oleogel increases its presence in the mixture, the flexural strength values increase, reaching in the case of the PP 10-25% mixture up to 98% in relation to the matrix.

In the case of the wood-based fillers, it can be determined that the particle diameter had a greater incidence on the flexural strength values than the chemical pre-treatment applied to the filler, reaching a value of 86% in relation to the matrix. The compounds with starch as filler have an average flexural strength value of 85% of the pure matrix value. However,

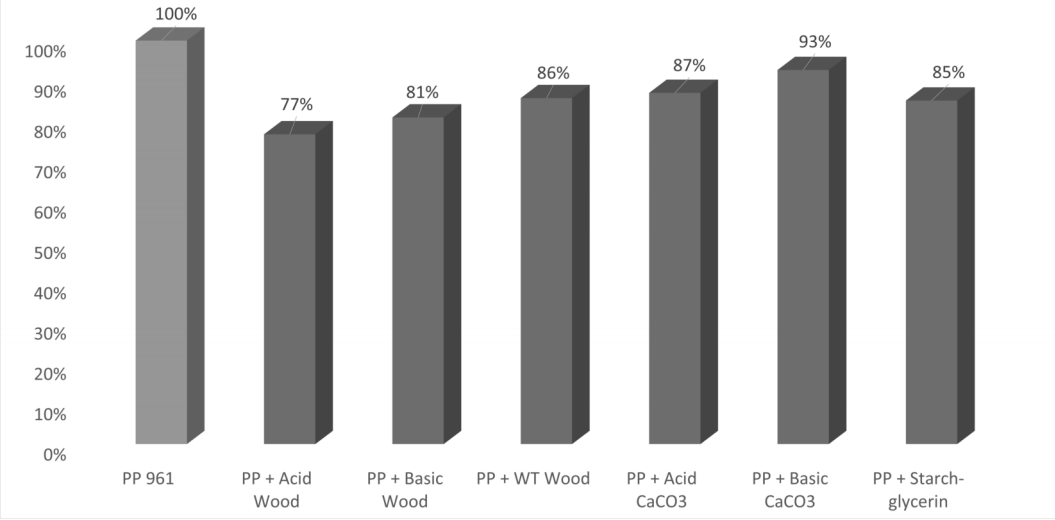

Figure 4.2: Flexural Strength Group

by looking closely at the individual values of each compound, it can be seen that for the PP + 10-30 Starch-Glycerin mixture, their Flexural strength values represent 80% of the value of the pure matrix, a value that is 10 percentage points below those in which the amount of plasticiser is half that of the pure matrix.

4.1.2 Tensile test

Table 4.2 shows the individual values of the mechanical properties obtained after uni-axial tensile tests of the composite materials. Composite materials that have been filled with wood in the matrix and chemically treated show yield stress values between 97 and 99% in relation to the pure matrix. This can be explained by the decrease of lignin in those wood composites that have received the chemical bath, action that allows them to break the micro cell walls to facilitated the dispersion of the microfibers of the filler within the matrix.

In the case of the composites with a mixture of chemically treated oleogel and $CaCO_3$ as dispersed phase, they present similar values of yield stress and are around 87% of the yield stress value of the pure matrix. Individually, it is observed that regardless of the chemical medium, acidic or basic, the composites that have a greater amount of oleogel present values closer to those of the pure material, as is the case of the specimens injected with PP + 10-25% $CaCO_3$ type material.

According to figure 4.3, it can be observed that the composites with natural fillers were the ones that obtained a performance closer to that of the pure matrix, whose yield strength value is 24.1 MPa. In the case of the starch-filled composites, their behaviour is equivalent to that of the pure matrix, and as in the flexural analysis, it can be observed that individually

Table 4.2: Tension Mechanical Test Result

Material	Mean Yield Strength (MPa)	STD Yield Strength (MPa)	Error (%)	Mean Young Modulus (%)	STD Young Modulus (%)	Error (%)	Mean Break Strain (%)	STD Break Strain (%)	Error (%)
PP 961	24.1	1.1	1.6	1452	178.5	4.3	228	35	5.4
PP + 5% WT Wood (300μ)	21.0	3.0	5.4	1798	238.4	5.0	23	3	4.9
PP+5% Acid Wood (500μ)	23.0	1.5	2.9	1456	155.3	4.8	25	4	5.5
PP + 10% Acid Wood (500μ)	23.9	1.4	2.7	1348	111.1	4.1	23	3	5.6
PP + 5% Basic Wood (500μ)	23.5	1.5	2.9	1500	181.9	5.4	26	3	5.2
PP + 10% Basic Wood (500μ)	24.5	0.7	1.6	1623	94.5	3.4	16	2	4.5
PP + 10-30% Starch-Glycerin	22.6	1.6	2.5	1458	210.0	5.1	21	3	5.7
PP + 10-15% Starch-Glycerin	25.6	2.9	5.1	1436	83.6	2.6	37	5	5.9
PP + 10-25% Acid CaCO3	19.7	1.7	3.4	1083	110.0	4.1	258	24	5.4
PP + 10-10% Acid CaCO3	20.3	1.1	2.2	1479	185.1	5.1	153	18	4.4
PP + 5-25% Acid CaCO3	22.6	0.3	0.5	1393	195.4	5.7	70	7	4.1
PP + 10-25% Basic CaCO3	22.8	0.8	1.4	1479	197.7	5.5	75	8	4.3
PP + 5-10% Acid CaCO3	21.4	1.1	2.1	1525	208.6	5.6	110	14	4.8
PP + 10-10% Basic CaCO3	20.7	0.7	1.3	1253	174.3	5.7	187	23	5.0
PP + 5-10% Basic CaCO3	19.0	0.2	0.5	1500	165.3	4.9	197	26	5.9
PP + 5-25% Basic CaCO3	21.5	0.8	1.6	1385	178.1	5.3	69	8	4.8

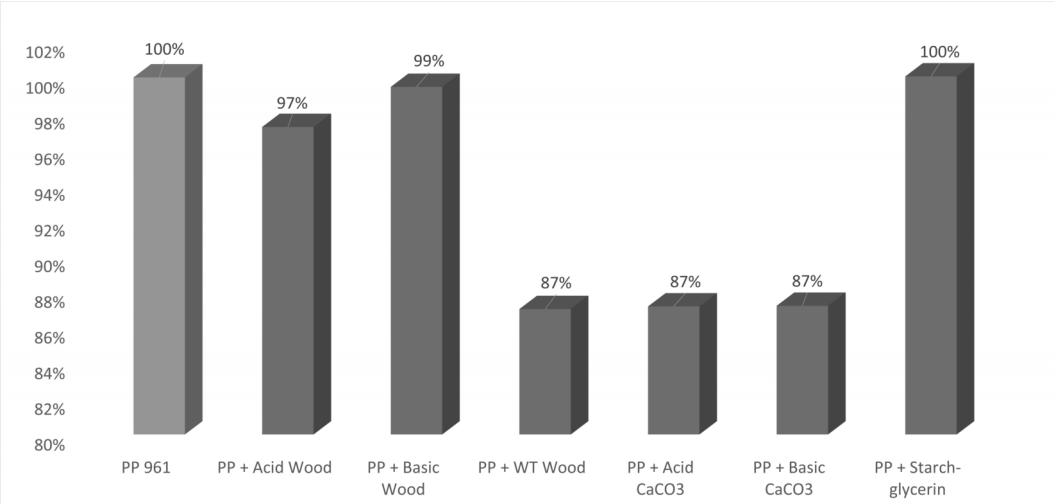

Figure 4.3: Yield Strength Group

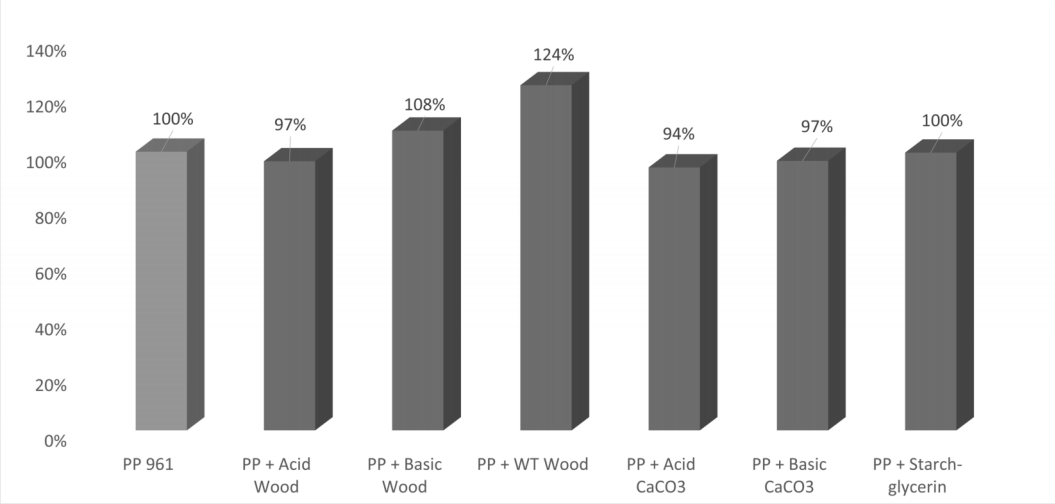

Figure 4.4: Young's Modulus Group

those specimens prepared with plasticiser material in greater proportion (30%) with respect to the filler were those that presented a lower performance, equal to 12 percentage points with respect to those with 15% glycerine in their preparation.

The Young's modulus of PP961 was defined as 1.45b GPa by the experimental procedures. According to the figure 4.4 it is observed that the composites containing as dispersed phase the wood particles without chemical treatment and with a particle diameter equal to 300μm are the ones that obtained a value 24% above the performance of the matrix. The composites containing the inorganic filler are those that present a lower yield than the pure matrix, having values of 6 and 3 percentage points below the same, being those that have a basic chemical pre-treatment the ones that are closer to the value of the pure PP.

The Young's modulus of PP961 was defined as 1.45b GPa by the experimental procedures. According to the figure 4.4 it is observed that the composites containing as dispersed phase the wood particles without chemical treatment and with a particle diameter equal to 300um are the ones that obtained a value 24% above the performance of the matrix.

The composites containing the inorganic filler are those that present a lower yield than the pure matrix, having values of 6 and 3 percentage points below the same, being those that have a basic chemical pre-treatment the ones that are closer to the value of the pure PP.

The break strain values can be seen in figure 4.5 show the highest variation between pure PP and the composites. Pure PP can withstand an elongation of up to 228% of its original length before breaking.The breakage itself presents a wide period of necking with the reduction of diameter. Compared to wood composites, the breakage occurred after an elongation of 10% of its initial length. A breakage that occurred in the form of tearing, with almost no necking in the breakage zone.

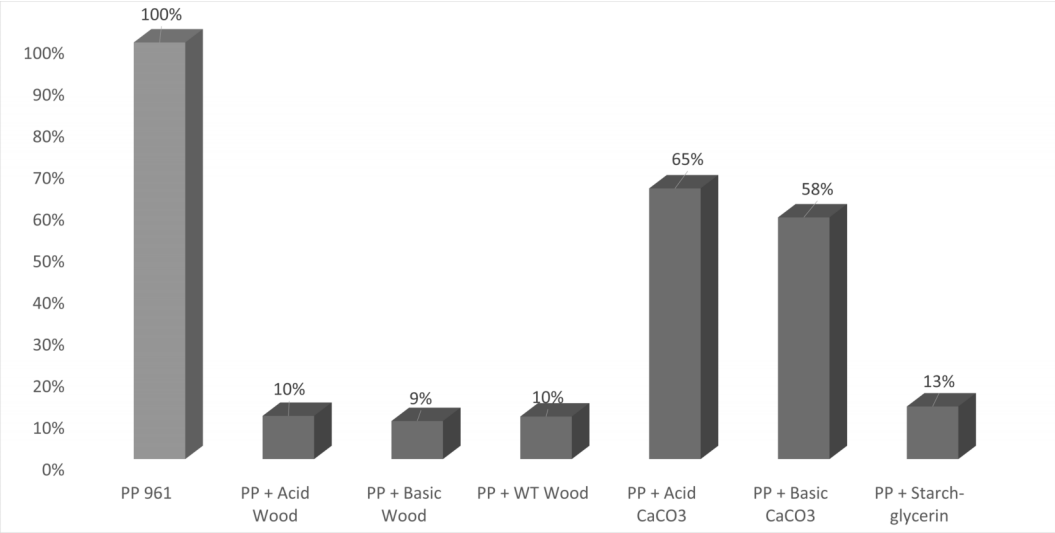

Figure 4.5: Break Strain Group Analysis

Wood filler composites that were prepared with a particle diameter of 300μm and without chemical pre-treatment presented a performance closer to the reference value of the pure matrix.

In the case of the composites to which a chemical pre-treatment was applied, as in the case of wood as calcium carbonate particles, those prepared in a basic medium showed a better performance, presenting an increase between 2 to 3% with respect to their counterparts in acid medium. This can be explained due to the chemical element used for the chemical conditioning of the basic medium, which was ammonium hydroxide. Ammonium salts have been reported to favour the cohesion between fillers and polymeric matrices by creating a coating film on the filler materials which allows the bonding between the linear polymer chains and their free radicals.

4.2 Thermogravimetric Analysis

The thermogravimetric analysis (TGA) of the composites was carried out in order to determine their melting and solidification temperature, as well as the latent enthalpy of these processes. The theoretical crystallinity of the composites was calculated and presented in table 4.3.

The difference in values between the melting and solidification temperature is the temperature range in which a material can be processed in an extrusion process such as the one involved in BAAM. In the composite materials that are the subject of this study, it can be observed that this temperature range is similar to that of the virgin material. A relevant data of this study is the calculation of the crystallinity of the composite materials in comparison

Table 4.3: Crystallinity and Thermal properties of composite materials

Material	Melting Temperature (ºC)	Entalphy of Fusion (ºC)	Solidification Temperature (ºC)	Entalphy Solidification J/g	Xc (%)
PP 961	134.8	239.7	113.0	-225.2	100
PP + 5% WT Wood (300μ)	136.4	237.1	114.3	-198.0	104
PP+5% Acid Wood (500μ)	136.0	147.5	113.6	-173.3	65
PP + 10% Acid Wood (500μ)	134.9	208.9	114.6	-245.8	97
PP + 5% Basic Wood (500μ)	137.4	147.4	113.5	-144.0	65
PP + 10% Basic Wood (500μ)	138.2	187.0	114.1	-164.1	87
PP + 10-30% Starch-Glycerin	136.9	148.6	113.6	-264.7	69
PP + 10-15% Starch-Glycerin	138.0	152.2	114.0	-224.8	71
PP + 10-25% Acid CaCO3	137.2	127.4	114.2	-252.4	59
PP + 10-10% Acid CaCO3	137.6	159.1	113.7	-219.2	74
PP + 5-25% Acid CaCO3	135.4	171.6	114.9	-215.8	75
PP + 10-25% Basic CaCO3	135.2	223.7	112.7	-202.6	104
PP + 5-10% Acid CaCO3	138.0	177.5	114.5	-261.9	78
PP + 10-10% Basic CaCO3	137.9	187.9	115.2	-233.7	87
PP + 5-10% Basic CaCO3	138.0	179.0	115.0	-225.2	79
PP + 5-25% Basic CaCO3	133.8	157.9	114.0	-206.3	69

with their matrix. This calculation is carried out by the following formula:

$$X_c(\%) = \frac{\Delta H_c}{\Delta H_m^{\circ}(1-x) * 100\%} \tag{4.1}$$

Where : X_c is the degree of crystallinity, ΔH_c is obtained by the melting peak area, $\Delta H^{\circ}m$ is the melting enthalpy of PP 961 100% crystalline, and x is filler weight fraction.

The cristallinity values calculated from TGA analysis are shown on figure 4.6. It can be seen that those compounds with chemical pretreatment are those with a lower value of crystallinity, a property that has an impact on the application of these materials in the BAAM process. A material with lower crystallinity presents lower shrinkage, this is explained by the special accommodation of the polymer chains at the moment of solidification.

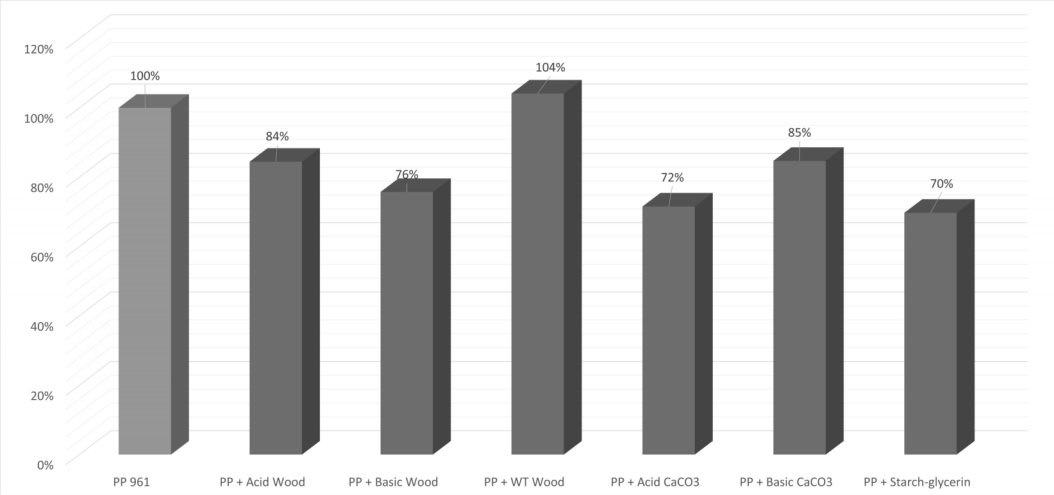

Figure 4.6: Crystallinity Composite Group

4.3 Temperature Analysis

The temperature profile of the BAAM process at different operating conditions was determined experimentally. Additionally, the experimental data was compared with a mathematical model proposed by Compton et al. [94], a model with which projections were made to determine the degree of incidence of different variables involved in the printing process.

The robotic arm was configured to print the geometry chosen for the analysis. Different deposition temperatures, bed temperature, speed and ambient temperature were tested, as indicated in table 4.4. Temperature values were obtained for different times, with which the figure 4.7 was generated. This was done with the use of an infrared thermometer of the brand Perel EEM100 set with an emissivity value of 0.87, located at a distance of no more than 1.5

m from the structure which was pointed at a specific point on the structure while it was being printed.

Table 4.4: BAAM Process Parameters

Configuration	T_deposition (°C)	T_bed (°C)	Speed (mm/s)	T_environment (°C)
1	170	110	150	22
2	200	110	175	22
3	185	90	135	22
4	170	45	135	22
5	170	110	175	140

Figure 4.7 shows a large temperature variation at the beginning of each curve, identified by temperature peaks with an almost constant amplitude, these intervals represent the addition of new filament layers within the printing process, which add heat to the system. After the printing period is the cooling process which is associated with a convection process, in which the fluid air comes in contact with the walls. This process is carried out in a natural way, or forced in the case of having an external source of air agitation. The cooling process runs more smoothly as can be seen in figure 4.7.

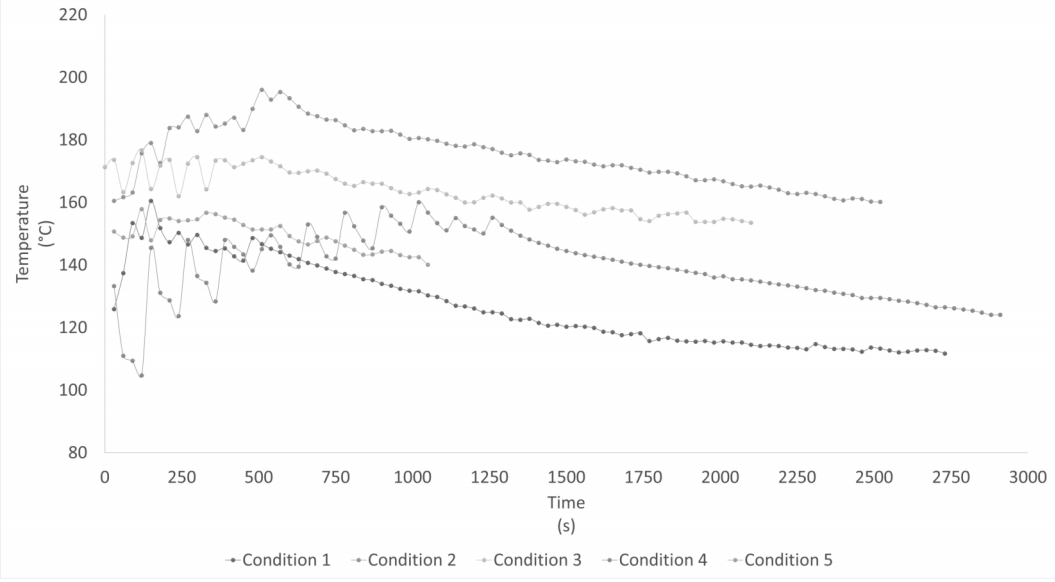

Figure 4.7: Temperature Profile at different printing conditions

It stands out from the figure 4.7 the beginning of the curve with the configuration 4, the one in which the temperature of the print bed is at room temperature. Here the temperature gradient is more evident, which gives an idea of the incidence that the bed temperature has in the decrease of temperature gradients that can trigger defects in the printed piece such as shrinkage and warping.

The comparison between configuration 2 and 3 revolves mainly around their difference in printing speeds. It is observed that the higher the speed the temperature gradients between the printed layers decrease, which is explained by the difference in the times between layers, allowing to increase the temperature of the lower layer that acts as a bed for the new filament layer. However, it can be observed that at the end of the printing time of configuration 2 there is a higher accumulated temperature peak. The risk that exists when increasing the speed is in not giving enough time for the lower layer to exceed the glass transition temperature, and being very liquid it does not provide the necessary support to not compromise the stability of the structure. As happened in several of the tests performed in this study.

In the case of controlled environments such as configuration 5, in which a heat source and turbulence source for the air was placed to increase the ambient temperature, very positive results were observed. Low temperature gradients can be observed in the figure 4.7 for configuration 5. Action performed mainly by decreasing the convection coefficients of the air, which decreases the rate of heat transfer in the system. This particular case simulates the closed environments currently used in small-scale AM printing.

Despite the good results presented by the heat addition in the system environment, it was not possible to effectively apply this configuration since only one fan was used to increase the air turbulence on only one wall of the printed part.

4.3.1 Modeling of Temperature

The mathematical model proposed by Compton[94], which describes the thermal process of construction by means of a 1D transient model, was applied. Different values for the parameters within the BAAM process were evaluated and the results shown below were obtained.

$$\dot{E}_{in} + \dot{E}_g = \dot{E}_{st} \tag{4.2}$$

The energy balance of equation 4.2 is considered as a starting point for the evaluation of the process. Here $\dot{E}_{in}$ indicates the amount of energy within the control volume, $\dot{E}_g$ represents the amount of energy generated within the control volume, which in this case for calculation simplification purposes is considered equal to zero. $\dot{E}_{st}$ is the energy stored inside the control volume.

In turn, the energy entering the control volume can be represented by its components, as shown in equation 4.3, where q_{cond} is conduction heat, q_{conv} is convection heat and q_{rad} is

the heat transferred to the system by radiation.

$$q_{cond} + q_{conv} + q_{rad} = \dot{E}_{st} \tag{4.3}$$

The heat of conduction for each of the temperature nodes is governed by equation 4.4.

$$q'_{cond} = \begin{cases} \frac{2kw}{\Delta x}(T_b - T_n^p) + \frac{kw}{\Delta x}(T_{n+1} - T_n^p), bottomnode \\ \frac{kw}{\Delta x}(T_{n-1} - T_n^p) + \frac{kw}{\Delta x}(T_{n+1} - T_n^p), middlenodes \\ \frac{kw}{\Delta x}(T_{n-1} - T_n^p), topnode \end{cases} \tag{4.4}$$

Figure 4.8 indicates the boundary conditions of the process and the values to be considered within equation 4.4

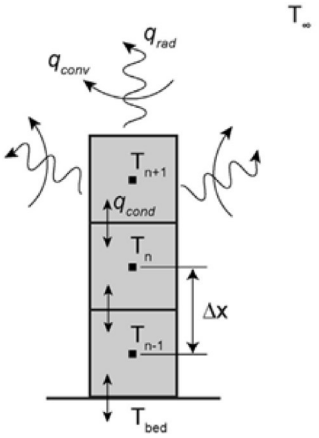

Figure 4.8: Boundary conditions thermal transfer [94]

$$q'_{cond} + q'_{rad} = \begin{cases} \Delta x(h + h_{rad})(T_\infty - T_n^p), bottomnode \\ 2\Delta x(h + h_{rad})(T_\infty - T_n^p), middlenodes \\ \Delta x(h + h_{rad})(T_\infty - T_n^p) + w(h + h_{rad})(T_\infty - T_n^p), topnode \end{cases} \tag{4.5}$$

$$\dot{E}'_{st} = \begin{cases} \frac{\rho c_p w}{\Delta t}\frac{\Delta x}{2}(T_n^{p+1} - T_n^p), bottom/topnode \\ \frac{\rho c_p w}{\Delta t}\Delta x(T_n^{p+1} - T_n^p), middlenodes \end{cases} \tag{4.6}$$

The equations 4.5 and 4.6 present the relationships for the calculation of convective heat, radiation and stored energy within the system.

The figure 4.9 shows how the temperature varies along the printing time in the BAAM

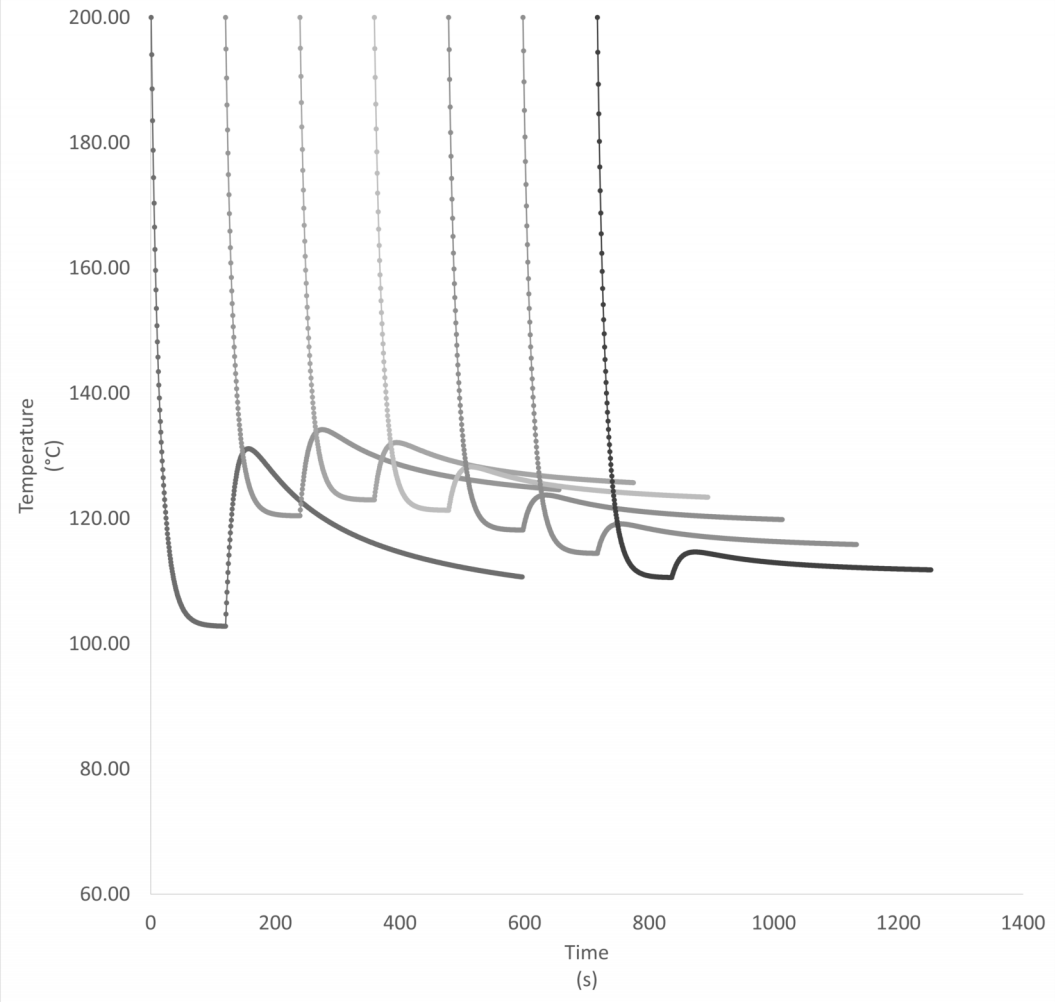

Figure 4.9: Temperature Profile, Mathematical Model

process for an interlayer time of 120s, a wall width of 25 mm, a wall height of 70 mm, a bed temperature of 110ºC, and a deposition temperature of 200ºC. It is observed that each entry of a new layer of filament generates an increase in temperature in the layer immediately below, an effect that is diminished as the number of printed layers increases.

The first printing layer is the one that experiences the highest temperature gradient, because it comes in contact with the bed temperature and its thermal equilibrium is controlled mainly by the conduction process between the metal base and the newly extruded filament layer. As the height of the structure increases the convection process between the surrounding air and the walls of the extruded piece is the predominant gradient of heat transfer, it is for this reason that from layer number 5 onwards the incidence of the bed temperature decreases and the upper layers begin to cool below the temperature of the previous layer seeking to reach the ambient temperature.

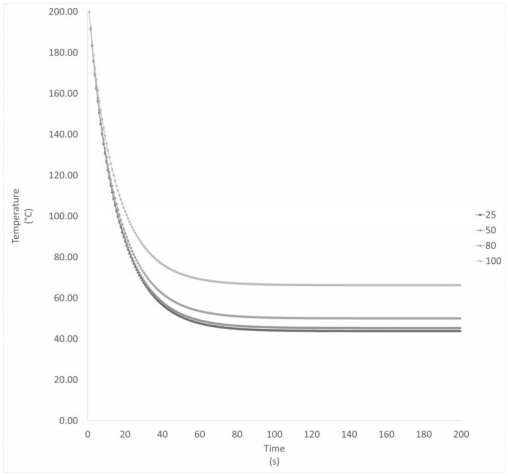

(a) Ambient temperature

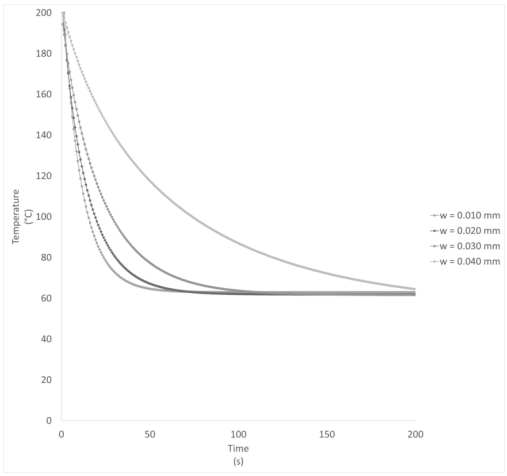

(b) Layer thickness

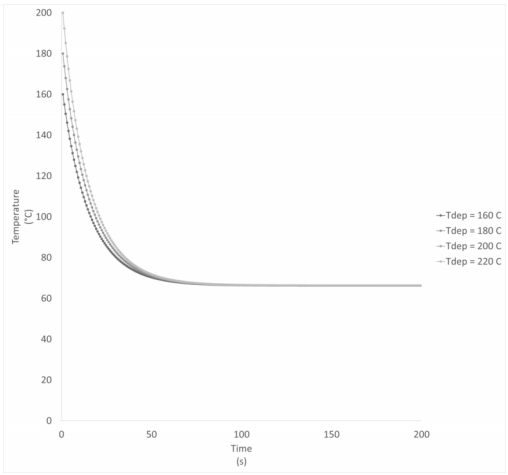

(c) Deposition temperature

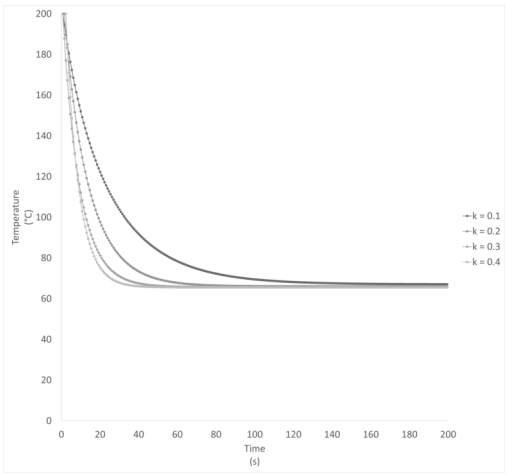

(d) Thermal conductivity of the material

Figure 4.10: Analysis of the effect of BAAM process parameters

The evaluation of different parameters within the BAAM process and its incidence in the final layer temperature is presented in the figure 4.10, final layer refers to those layers that are above the ones where the bed temperature has incidence. The proportion of time it takes for the freshly printed layer to reach its solidification temperature is evaluated, after which time fractures will occur in the structure if the next layer is not deposited.

Figure 4.10 indicates that the variable that has the greatest impact on the prevention of fractures caused by lack of cohesion between printed laminates is the layer thickness. An increase in the time it takes for the material to reach its solidification temperature is observed as the layer width increases, which is mainly explained by the amount of heat stored inside the lower layers resulting in a higher base temperature, a factor that directly affects the conductivity coefficient, reducing its heat transfer gradient. In the case of shapes with more complex geometries than those executed in this project, it is anticipated that it will be nec-

essary to pay particular attention to those areas where there is narrowing or changes in the velocity of printing.

After the layer thickness, the most important factor is the environment temperature. Considering that this is BAAM, it is complex to control environmental conditions when the process is carried out outside of a closed chamber. However, this effect is accentuated for ambient temperatures close to the solidification temperature, otherwise the incidence is not considered appreciable.

Finally, a factor that presents a negative correlation is the conductivity coefficient, which, by decreasing its value, increases the time it takes for the system to reach the solidification temperature. Effect generated by the decrease of the conductivity coefficient between the layers, by hindering the heat transfer. The effect of the fillers inside the polymeric matrix is shown by the increase of the thermal conductivity.

It is necessary to indicate that being the BAAM process multivariate, this model represents partially and in a simplified way the behavior of the process to different operating conditions, nevertheless it presents a good approximation and it is useful for the evaluation of future scenarios, mainly for composite materials in which the physico-chemical properties of the materials are not widely disclosed.

4.4 Dimensional and Geometric Analysis

4.4.1 Deviation Analysis

The deviation analysis of BAAM printed geometries between composite materials and pure PP961, as well as the warpage values, is presented.

The geometry of the printed parts was captured using a 3D scan, with the data collected using CloudCompare software. A deviation analysis was performed between the geometry obtained for the PP961 seen in figure 4.11a, represented in white color, and its composite derivatives calcium carbonate and starch filler composite as seen in figure 4.11c and 4.11b respectively. The scalar field with a range between -10 and +10, represented by blue and red at its extremes respectively, presents the distance between the evaluated pieces in relation to their reference points, being the green color the tone that indicates greater closeness to it.

It should be noted that during the scanning process it was not possible to collect all the values of the physical element, either due to overlapping layer of materials or due to limitation of the data collection equipment. Because of this the deviation values between the geometry of the samples and their reference values do not present a mathematically representative

(a) Polypropylene Matrix PP961 **(b)** Starch Printed Composite **(c)** $CaCo_3$ Printed Composite

Figure 4.11: Comparison between pure matrix and filler composite of Starch and Calcium Carbonate

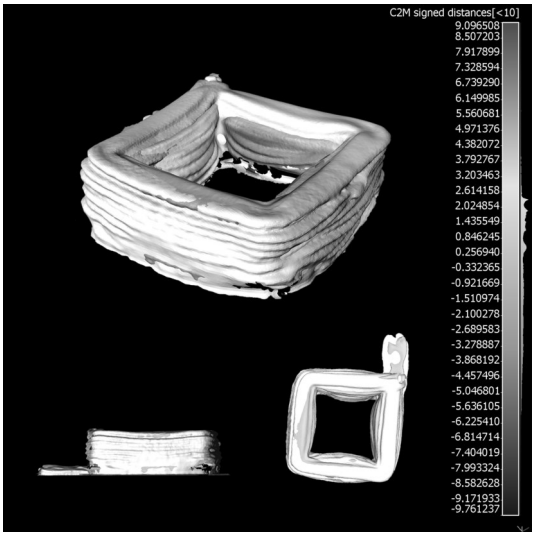

Figure 4.12: Deviation Analysis of Calcium Carbonate filler Composite

value. However, their closeness or remoteness to the reference standard can be appreciated in a qualitative way.

The part printed with calcium carbonate as filler, presents geometrically a good approximation with the standard as shown in figure 4.12. In the external edges the concordance is almost total, while in the internal part is where the biggest deviation is presented. This effect is mainly generated by the increase in the density of the composite material and the longer cooling time required by the material, which is why, when maintaining the printing speed used in the reference standard, the lower layers were at a point of fluidity that compromised the stability of the structure.

Figure 4.13 shows a poor approximation for parts printed with starch fillers. The main problem that occurred during the extrusion of the material was the failure to generate a continuous filament, which totally compromised the geometry of the part. The presence of lumps inside the filament was the reason for the described problem, this defect was due to the process chosen for the preparation of the composite materials in which the starch moisture was not adequately removed.

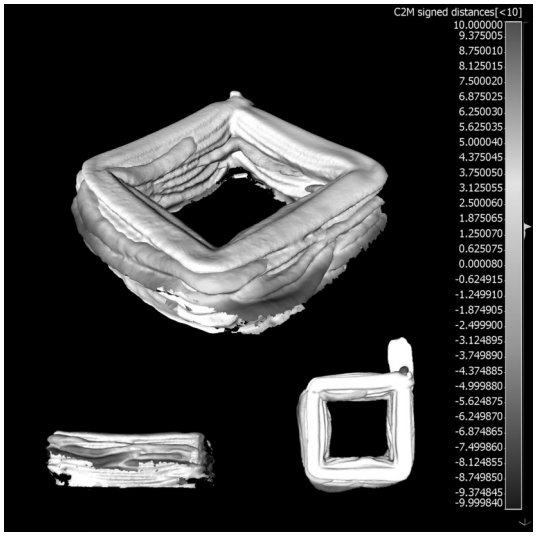

Figure 4.13: Deviation Analysis of Starch Filler Composite

The wood fillers as seen in 4.14c generated a sponge-like structure with a regular approximation to the geometry presented by the matrix. The lower corners showed the greatest deviation, due to the warping of the structure and the variation of the bead width along the structure. Poor interlayer cohesion was evidenced along with processability problems.

Additionally, the BAAM process was also tested with PP Repsol, supplied from another brand (as shown in figure 4.14a) and GF Composite (as seen in figure) 4.14b using the defined conditions to evaluate the impact of the matrix on the results obtained.

Figures 4.15 and 4.16 show the deviations of the printed samples in relation to the PP961 used as matrix of the composite materials prepared in this study. In red is marked in both cases the deviation presented in the lower part of the printed pieces, this due to the little or no warping of the printed pieces. It is observed that the geometry of both structures is quite close to that designed in the CAD model, presenting a higher performance than that obtained with the PP961 material.

4.4.2 Warpage

Figure 4.17 and 4.18 shows the different printed parts and their different degrees of warp in relation to the horizontal reference plane.

Table 4.5 shows the values obtained after measuring the separation between the corners of the printed material and its horizontal reference plane. The starch composites are the ones that presented the highest warpage value, having 8 percent above the value of the matrix.

(a) PP Pure Matrix Repsol **(b)** PP with Glass Fiber **(c)** PP with Wood Filler

Figure 4.14: Comparison between pure matrix(left) and filler composite - glass fiber (center) and wood (right)

Figure 4.15: Deviation Analysis of Glass Fiber Composite

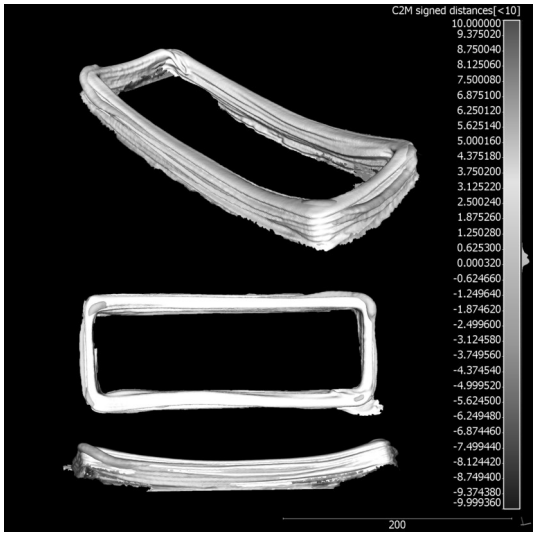

Figure 4.16: Deviation Analysis of Wood Filler Composite

(a) Pure PP **(b)** Starch Filler Composite **(c)** $CaCO_3$ Filler Composite

Figure 4.17: Warping Analysis Set 1

(a) Pure PP **(b)** Glass Fiber Composite **(c)** Wood Filler Composite

Figure 4.18: Warping Analysis Set 2

Table 4.5: Warping in printed parts for BAAM

Material	Warpage (mm)	STD	Error (%)	Comparison Ratio (%)
PP961	21.49	2.58	5.4	100
PP Calcium Carbonate	19.11	2.15	5.04	89
PP 30GF	<5	-	-	
PP Repsol	17.3	1.74	4.49	81
PP Wood	21.07	1.95	4.16	98
PP Starch	23.22	2.16	4.17	108

The values for PP 30GF were not recorded because of the lack of precision in the reported values due to the limitations of the measuring element, which in all cases were less than 5 mm. The polypropylene from the manufacturer Repsol presents a lower warpage with the same operating conditions used for the case of PP961 within the BAAM process.

5 Conclusions and Future Works

In this chapter the most relevant findings of the results are presented, regarding the feasibility of processing the composite materials analyzed in this study for their application in the Big Area Additive Manufacturing process. In addition, future work has been suggested related to the topic raised.

5.1 Conclusion

According to the results obtained after the experimental tests carried out on the composite materials object of this study, the following conclusions could be drawn:

The processability of three different composite materials manufactured with the same matrix for implementation in the BAAM process was tested. The pH of the medium in which the fillers were pre-treated showed to have an effect on the thermal and mechanical properties of the composites obtained, with the basic medium showing the best results in general.

The composites with sawdust as filler material showed the closest mechanical properties to the matrix, with a proximity value of 97%. The diameter of the particle material was the factor with the highest incidence for this result, over the chemical pre-treatment. The processability of these materials within the BAAM process was below the reference values, presenting higher warpage and geometrical deviation.

The composites with calcium carbonate filler were the ones that presented better performance in the BAAM printing process, a lower warpage and geometric deviation, effects associated with the higher thermal resistance of the filler and the decrease in the crystallinity of the composite.

In general for the potato starch composites, those with 15% plasticiser in relation to the amount of filler in the mixture showed better mechanical response than those with 30%.

The temperature of the print bed was the one that presented the greatest incidence in the manufacture of parts using BAAM, a parameter that is mainly important in the first 6 or 7 layers of the structure as evidenced by the Compton mathematical model, ratified in this study. After this point the prevailing factor is the temperature of the environment.

5.2 Future works

Recommendations for future work are presented to further develop the state of the art of composite materials based on secondary raw materials for use in BAAM.

- Evaluation of different levels of chemical concentration media for the pre-treatment of fillers and their impact on the mechanical and thermal properties of the composites.
- Evaluation of the impact of chemical solution baths on the processability and mechanical response of recycled plastic materials. Example of saline water in plastics recovered from the sea.

Bibliography

[1] P Krawczak. “Additive manufacturing of plastic and polymer composite parts: Promises and challenges of 3D-printing”. In: *Express Polymer Letters* 9.11 (2015), pp. 959–959.

[2] ASTM Committee F42 on Additive Manufacturing Technologies and ASTM Committee F42 on Additive Manufacturing Technologies. Subcommittee F42. 91 on Terminology. *Standard terminology for additive manufacturing technologies*. Astm International, 2012.

[3] Chad E Duty et al. “Structure and mechanical behavior of Big Area Additive Manufacturing (BAAM) materials”. In: *Rapid Prototyping Journal* (2017).

[4] Nathalie Labonnote et al. “Additive construction: State-of-the-art, challenges and opportunities”. In: *Automation in construction* 72 (2016), pp. 347–366.

[5] Eric Barnett and Clément Gosselin. “Large-scale 3D printing with a cable-suspended robot”. In: *Additive Manufacturing* 7 (2015), pp. 27–44.

[6] Nayanee Gupta, Christopher Weber, and Sherrica Newsome. “Additive manufacturing: status and opportunities”. In: *Science and Technology Policy Institute, Washington* (2012).

[7] Mohsen Ziaee and Nathan B Crane. “Binder jetting: A review of process, materials, and methods”. In: *Additive Manufacturing* 28 (2019), pp. 781–801.

[8] Yun Bai and Christopher B Williams. “An exploration of binder jetting of copper”. In: *Rapid Prototyping Journal* (2015).

[9] TA Grimm et al. “3D Printer Benchmark: North American Edition”. In: *TA Grimm & Associates Inc, www. tagrimm. com* (2010).

[10] Ian Gibson, David Rosen, and Brent Stucker. “Directed energy deposition processes”. In: *Additive manufacturing technologies*. Springer, 2015, pp. 245–268.

[11] *Electron Beam Additive Manufacturing (EBAM®)*. URL: https://www.sciaky.com/additive-manufacturing/electron-beam-additive-manufacturing-technology.

[12] Jamison Go and A John Hart. “Fast desktop-scale extrusion additive manufacturing”. In: *Additive Manufacturing* 18 (2017), pp. 276–284.

[13] *F900 3D Printers for Large Build Manufacturing*. URL: https://www.stratasys.com/3d-printers/stratasys-f900.

[14] Ian Gibson et al. “Material Jetting”. In: *Additive Manufacturing Technologies*. Springer, 2021, pp. 203–233.

[15] Ian Gibson et al. “Vat Photo Polymerization”. In: *Additive Manufacturing Technologies*. Springer, 2021, pp. 77–121.

[16] *ProX 950*. Jan. 2021. URL: https://www.3dsystems.com/3d-printers/prox-950.

[17] Rajkumar Velu, Dhileep Kumar Jayashankar, and Karupppasamy Subburaj. “Additive processing of biopolymers for medical applications”. In: *Additive Manufacturing*. Elsevier, 2021, pp. 635–659.

[18] Riya Singh et al. “Powder bed fusion process in additive manufacturing: An overview”. In: *Materials Today: Proceedings* 26 (2020), pp. 3058–3070.

[19] *SLM®800*. Jan. 2021. URL: https://www.slm-solutions.com/products-and-solutions/machines/slm-800/.

[20] Neil Hopkinson, RJM Hague, PM Dickens, et al. “Rapid manufacturing”. In: *An Industrial Revolution for the Digital Age. Chichister, England: John Wiley and Sons, Ltd* (2006).

[21] Ana Pilipovic et al. “Laminate object manufacturing Vs. Fused deposition modeling-machine comparison”. In: *Annals of DAAAM and Proceedings of the International DAAAM Symposium*. Vol. 22. 1. DAAAM Vienna, Austria. 2011, pp. 221–222.

[22] Hamad Al Jassmi, Fady Al Najjar, and Abdel-Hamid Ismail Mourad. “Large-Scale 3D printing: the way forward”. In: *IOP Conference Series: Materials Science and Engineering*. Vol. 324. 1. IOP Publishing. 2018, p. 012088.

[23] Behrokh Khoshnevis et al. “Crafting large prototypes”. In: *IEEE Robotics & Automation Magazine* 8.3 (2001), pp. 33–42.

[24] Behrokh Khoshnevis. “Automated construction by contour crafting—related robotics and information technologies”. In: *Automation in construction* 13.1 (2004), pp. 5–19.

[25] Paul Bosscher et al. “Cable-suspended robotic contour crafting system”. In: *Automation in construction* 17.1 (2007), pp. 45–55.

[26] Joseph Pegna. “Exploratory investigation of solid freeform construction”. In: *Automation in construction* 5.5 (1997), pp. 427–437.

[27] F Ceccanti et al. “3D printing technology for a moon outpost exploiting lunar soil”. In: *61st International Astronautical Congress, Prague, CZ, IAC-10-D3*. Vol. 3. 2010, pp. 1–9.

[28] Aant van der Zee, Paul de Ruiter, and Hayo Meijs. “Unleash the building bots: 3d printing structures with an autonomous robot swarm”. In: *SPOOL* 4.2 (2017), pp. 65–67.

[29] Dongping Deng and Yong Chen. “An origami inspired additive manufacturing process for building thin-shell structures”. In: *ASME International Mechanical Engineering Congress and Exposition*. Vol. 56185. American Society of Mechanical Engineers. 2013, V02AT02A016.

[30] Prahar M Bhatt et al. “Expanding capabilities of additive manufacturing through use of robotics technologies: A survey”. In: *Additive Manufacturing* 31 (2020), p. 100933.

[31] Charles Hill et al. *Big Area Additive Manufacturing (BAAM) Materials Development and Reinforcement with Advanced Composites*. Tech. rep. Inst. for Advanced Composites Manufacturing Innovation (IACMI), Knoxville . . ., 2018.

[32] Chad E Duty, Tom Drye, and Alan Franc. *Material development for tooling applications using big area additive manufacturing (BAAM)*. Tech. rep. Oak Ridge National Lab.(ORNL), Oak Ridge, TN (United States). Manufacturing . . ., 2015.

[33] Lonnie J Love et al. *Breaking barriers in polymer additive manufacturing*. Tech. rep. Oak Ridge National Lab.(ORNL), Oak Ridge, TN (United States). Manufacturing . . ., 2015.

[34] Halil L Tekinalp et al. "Highly oriented carbon fiber–polymer composites via additive manufacturing". In: *Composites Science and Technology* 105 (2014), pp. 144–150.

[35] Lonnie J Love et al. "The importance of carbon fiber to polymer additive manufacturing". In: *Journal of Materials Research* 29.17 (2014), pp. 1893–1898.

[36] Lonnie J Love and Chad Duty. "Cincinnati big area additive manufacturing (BAAM)". In: *Oak Ridge, TN* (2015).

[37] Kinjal Gandha et al. "Additive manufacturing of anisotropic hybrid NdFeB-SmFeN nylon composite bonded magnets". In: *Journal of Magnetism and Magnetic Materials* 467 (2018), pp. 8–13.

[38] L Pigliaru et al. "3D printing of high performance polymer-bonded PEEK-NdFeB magnetic composite materials". In: *Functional Composite Materials* 1 (2020), pp. 1–17.

[39] Ian Gibson et al. "Design for additive manufacturing". In: *Additive manufacturing technologies*. Springer, 2021, pp. 555–607.

[40] Alex Roschli et al. "Designing for big area additive manufacturing". In: *Additive Manufacturing* 25 (2019), pp. 275–285.

[41] Omer EYERCIOGLU et al. "Determination of The Maximum Bridging Distance in Large Scale Additive Manufacturing". In: *4th International Congress on 3d Printing (Additive Manufacturing) Technologies and Digital Industry*, pp. 40–48.

[42] Eduardo José Custódio Branquinho Crespo. "Parametrização do Fabrico Aditivo em Grande Escala por FDM". MA thesis. 2019.

[43] Gaurav Ameta et al. "Investigating the role of geometric dimensioning and tolerancing in additive manufacturing". In: *Journal of Mechanical Design* 137.11 (2015).

[44] Phillip Chesser et al. "Extrusion control for high quality printing on Big Area Additive Manufacturing (BAAM) systems". In: *Additive Manufacturing* 28 (2019), pp. 445–455.

[45] J Shah et al. "Large-scale 3D printers for additive manufacturing: design considerations and challenges". In: *The International Journal of Advanced Manufacturing Technology* 104.9 (2019), pp. 3679–3693.

[46] John Samuel Batchelder and Steven Scott Crump. *Method for rapid prototyping of solid models*. US Patent 5,866,058. Feb. 1999.

[47] Brian K Post et al. *Feasibility of using big area additive manufacturing to directly manufacture boat molds*. Tech. rep. Oak Ridge National Lab.(ORNL), Oak Ridge, TN (United States), 2018.

[48] Brian Post et al. *Additive Manufacturing of Wind Turbine Molds*. Tech. rep. Oak Ridge National Lab.(ORNL), Oak Ridge, TN (United States), 2017.

[49] Bradley S Richardson, Mark W Noakes, and Alex C Roschli. *BAAM Additive Manufacturing of Magnetically Levitated Wind Turbine*. Tech. rep. Oak Ridge National Lab.(ORNL), Oak Ridge, TN (United States), 2018.

[50] Lonnie Love et al. *Feasibility of Using BAAM for Mold Inserts for the Precast Concrete Industry*. Tech. rep. Oak Ridge National Lab.(ORNL), Oak Ridge, TN (United States), 2019.

[51] Ling Li et al. "Big area additive manufacturing of high performance bonded NdFeB magnets". In: *Scientific reports* 6.1 (2016), pp. 1–7.

[52] Andrzej Nycz et al. *Development and Demonstration of Large-Scale Metal Additive Manufacturing for Military Vehicle Applications-Final Report*. Tech. rep. Oak Ridge National Lab.(ORNL), Oak Ridge, TN (United States), 2019.

[53] Scott Curran et al. *Big area additive manufacturing and hardware-in-the-loop for rapid vehicle powertrain prototyping: A case study on the development of a 3-D-printed Shelby Cobra*. Tech. rep. SAE Technical Paper, 2016.

[54] Brian K Post et al. *Additive Manufacturing of Tooling for Refrigeration Cabinet Foaming Processes*. Tech. rep. Oak Ridge National Lab.(ORNL), Oak Ridge, TN (United States). Manufacturing …, 2016.

[55] Michelle M Gauthier. *Engineered materials handbook*. Vol. 1. ASM International, 1995.

[56] Güneri Akovali. *Handbook of composite fabrication*. iSmithers Rapra Publishing, 2001.

[57] Charles A Harper. *Handbook of plastics, elastomers, and composites*. McGraw-Hill Education, 2002.

[58] Moby Ahmed. *Glass-reinforced, Recycled PET as Additive Manufacturing Feedstock*. Tech. rep. Ambercycle, Inc. Mesa United States, 2019.

[59] Camden A Chatham et al. "Extrusion additive manufacturing of semi-crystalline PET/PP blends". In: *2018 Society of Plastics Engineers Annual Technical Conference, ANTEC 2018*. 2018.

[60] Karthikeyan Gnanasekaran et al. "3D printing of CNT-and graphene-based conductive polymer nanocomposites by fused deposition modeling". In: *Applied materials today* 9 (2017), pp. 21–28.

[61] Andrew N Dickson et al. "Fabrication of continuous carbon, glass and Kevlar fibre reinforced polymer composites using additive manufacturing". In: *Additive Manufacturing* 16 (2017), pp. 146–152.

[62] AA Stepashkin et al. “3D-printed PEEK-carbon fiber (CF) composites: Structure and thermal properties”. In: *Composites Science and Technology* 164 (2018), pp. 319–326.

[63] Nicolas Mys. “Processing and characterization of polymeric materials to spherical powders as candidate build material for fusion based additive manufacturing”. PhD thesis. Ghent University, 2017.

[64] Peng Liu et al. “Rheology, crystal structure, and nanomechanical properties in large-scale additive manufacturing of polyphenylene sulfide/carbon fiber composites”. In: *Composites Science and Technology* 168 (2018), pp. 263–271.

[65] S Syngellakis. *Natural Filler and Fibre Composites: Development and Characterisation*. Vol. 87. WIT Press, 2015.

[66] Sun-M Lai et al. “Comparative study of maleated polyolefins as compatibilizers for polyethylene/wood flour composites”. In: *Journal of Applied Polymer Science* 87.3 (2003), pp. 487–496.

[67] Silvia HP Bettini et al. “Effect of sawdust surface treatment and compatibilizer addition on mechanical behavior, morphology, and moisture uptake of polypropylene/sawdust composites”. In: *Polymer Engineering & Science* 50.5 (2010), pp. 978–985.

[68] Shan Jin and Laurent M Matuana. “Coextruded PVC/wood-flour composites with WPC cap layers”. In: *Journal of Vinyl and Additive Technology* 14.4 (2008), pp. 197–203.

[69] Koay S Chun et al. “Wood-plastic composites made from corn husk fiber and recycled polystyrene foam”. In: *J. Eng. Sci. Technol* 13.11 (2018), pp. 3445–3456.

[70] Rudolph D Deanin and Nick R Schott. *Fillers and reinforcements for plastics*. ACS Publications, 1974.

[71] Muralisrinivasan Natamai Subramanian. *Polymer Blends and Composites: Chemistry and Technology*. John Wiley & Sons, 2017.

[72] Nicolas Brosse, Mohd Hazwan Hussin, and Afidah Abdul Rahim. “Organosolv processes”. In: *Biorefineries* (2017), pp. 153–176.

[73] Seyed Mohammad Mirmehdi, GUSTAVO HENRIQUE DENZIN TONOLI, and Fatemeh Dabbagh. “Lignocellulose-polyethylene composite: influence of delignification, filler content and filler type”. In: *Cellulose Chemistry and Technology* 51.3-4 (2017), pp. 341–346.

[74] Yao Chen et al. “Thermal behavior of extracted and delignified pine wood flour”. In: *Thermochimica Acta* 591 (2014), pp. 40–44.

[75] Athanasios Dimitriou, MD Hale, and MJ Spear. “The effect of pH on surface activation of wood polymer composites (WPCs) with hydrogen peroxide for improved adhesion”. In: *International Journal of Adhesion and Adhesives* 85 (2018), pp. 44–57.

[76] D Byrom. “Miscellaneous biomaterials”. In: *Biomaterials*. Springer, 1991, pp. 333–359.

[77] NG Olaiya et al. “Properties and characterization of a PLA–chitin–starch biodegradable polymer composite”. In: *Polymers* 11.10 (2019), p. 1656.

[78] EM Khar'kova et al. "Starch–polyethylene polymer–polymer composites obtained by polymerization filling: Structure and oxidative degradability". In: *Polymer Science, Series B* 59.5 (2017), pp. 601–609.

[79] Caroline Baillie. *Green composites: polymer composites and the environment*. CRC Press, 2005.

[80] V Volpe et al. "Use of sunflower seed fried oil as an ecofriendly plasticizer for starch and application of this thermoplastic starch as a filler for PLA". In: *Industrial Crops and Products* 122 (2018), pp. 545–552.

[81] Joemer A Adorna et al. "Effect of Lauric Acid on the Thermal and Mechanical Properties of Polyhydroxybutyrate (PHB)/Starch Composite Biofilms". In: *International Journal of Polymer Science* 2020 (2020).

[82] Klaudia Piekarska, Ewa Piorkowska, and Joanna Bojda. "The influence of matrix crystallinity, filler grain size and modification on properties of PLA/calcium carbonate composites". In: *Polymer Testing* 62 (2017), pp. 203–209.

[83] Guijun Yang, Young-Jung Heo, and Soo-Jin Park. "Effect of morphology of calcium carbonate on toughness behavior and thermal stability of epoxy-based composites". In: *Processes* 7.4 (2019), p. 178.

[84] Achanai Buasri et al. "Thermal and mechanical properties of modified CaCO3/PP nanocomposites". In: *Int. J. Chem. Mol. Nucl. Mater. Metall. Eng* 6.8 (2012), p. 2012.

[85] Slavica R Mihajlović et al. "Mechanism of stearic acid adsorption to calcite". In: *Powder technology* 245 (2013), pp. 208–216.

[86] Zhi Cao et al. "Chemical surface modification of calcium carbonate particles with stearic acid using different treating methods". In: *Applied Surface Science* 378 (2016), pp. 320–329.

[87] Peter Kiss et al. "An experimental study of glass fibre roving sizings and yarn finishes in high-performance GF-PA6 and GF-PPS composite laminates". In: *Composites Part B: Engineering* 204 (2021), p. 108487.

[88] Galal Sherif et al. "Effect of glass fibers thermal treatment on the mechanical and thermal behavior of polysulfone based composites". In: *Polymers* 12.4 (2020), p. 902.

[89] Alessandro Pegoretti. "Recycling concepts for short-fiber-reinforced and particle-filled thermoplastic composites: a review". In: *Advanced Industrial and Engineering Polymer Research* (2021).

[90] D ASTM. "Standard Test Method for Melt Flow Rates of Thermoplastics by Extrusion Plastometer". In: *ASTM D1238-13* (2013).

[91] Matthias Wagner. *Thermal analysis in practice: fundamental aspects*. Carl Hanser Verlag GmbH Co KG, 2017.

[92] Ashley Clarke, Colin Eberhardt, and Colin Nigel Eberhardt. *Microscopy techniques for materials science*. Woodhead Publishing, 2002.

[93] David Julian McClements et al. “Lipid-based emulsions and emulsifiers”. In: *Food lipids: Chemistry, nutrition, and biotechnology* 3 (2008), pp. 63–98.

[94] Brett G Compton et al. “Thermal analysis of additive manufacturing of large-scale thermoplastic polymer composites”. In: *Additive Manufacturing* 17 (2017), pp. 77–86.

Appendices

Appendix A - Wood delignification and partial crystallization procedures

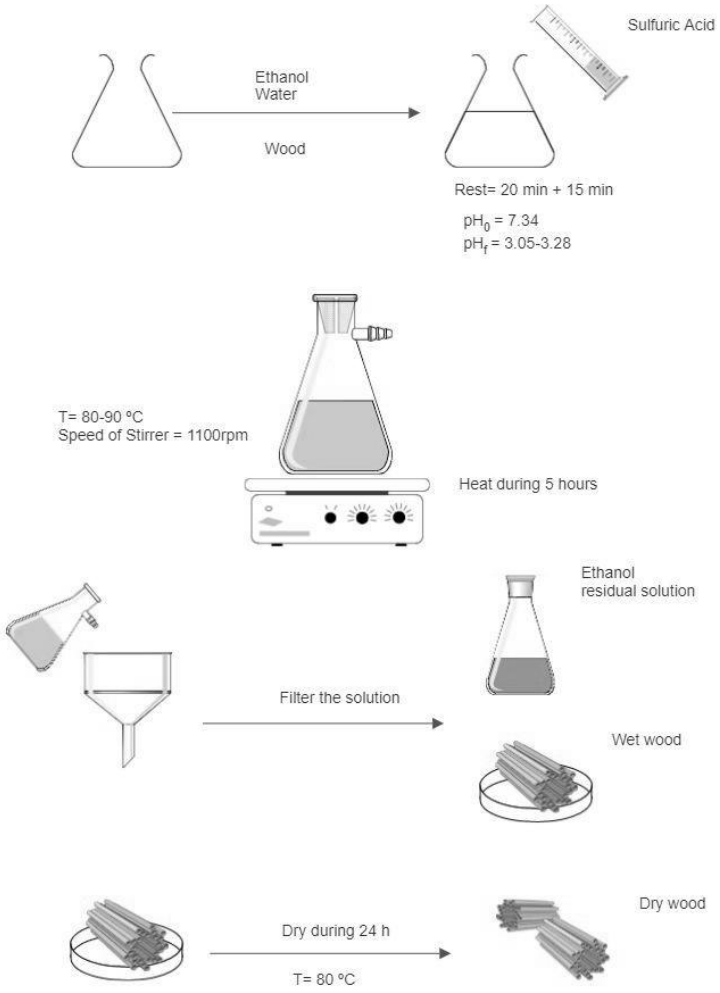

Figure 5.1: Sawdust Pretreatment

Delignification Process Each element was weighed separately before it was used in the reaction. The ethanol was placed in a flask, the wood was immersed in the flask with the ethanol and, it was left to rest for 20 minutes while the sawdust was totally moistened. The initial pH of the wood plus ethanol was measured, which showed a value of 7.34. The indicated amount of sulfuric acid (for acid) / Ammonium Hydroxide (for basic) was added to reach an acid point equal to 3.05. The mixture was left to stand again for its homogenization for 15 minutes more. The mixture was heated under controlled conditions of temperature (80-90ºC) and agitation (1100 rpm) for 5 hours. It was cooled, then filtered to separate the solids and the residual solution that was not evaporated during the process. The residual solution was discarded, and the filtered wet wood was placed in a stove to dehydrated it for 24 hours at a controlled temperature of 80ºC.

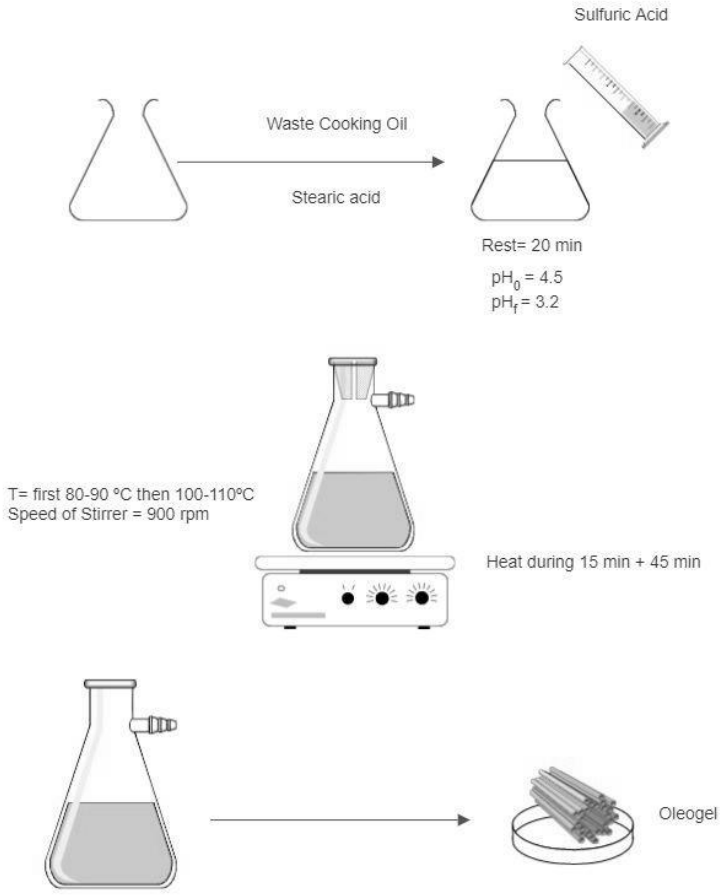

Figure 5.2: Oleogel Preparation

Partial Crystallization Each element was weighed separately before it was used in the reaction. The waste cooking oil was placed in a flask together with the defined amount of stearic acid. The initial pH of the waste cooking oil plus stearic acid was measured, which showed a value of 4.5. The indicated amount of sulfuric acid (for acid) / Ammonium Hydroxide (for basic) was added to reach a basic point equal to 3.2(acid)/10.2(basic) The mixture was left to rest to its homogenization for 20 minutes. The mixture was heated under controlled conditions of temperature (80-90ºC) and agitation (900 rpm) for 15 min. Then the temperature was increased until the range of 100-110 ºC to remove the moisture of the oil, the heating process was continued until reach 60 min of reaction. The oleo gel mixture was cooled, then removed from the flask.